NASA CR-54245
GDA-DBE 64-052-4

DEVELOPMENT OF A COAXIAL PLASMA GUN FOR SPACE PROPULSION

by
Terence J. Gooding, Alan V. Larson,
Bruce R. Hayworth, and David E. T. F. Ashby

Prepared for
NATIONAL AERONAUTICS AND SPACE ADMINISTRATION

CONTRACT NAS 3-5759

GENERAL DYNAMICS
Convair Division
San Diego, California

NOTICE

This report was prepared as an account of Government sponsored work. Neither the United States, nor the National Aeronautics and Space Administration (NASA), nor any person acting on behalf of NASA:

A.) Makes any warranty or representation, expressed or implied, with respect to the accuracy, completeness, or usefulness of the information contained in this report, or that the use of any information, apparatus, method or process disclosed in this report may not infringe privately owned rights; or

B.) Assumes any liabilities with respect to the use of, or for damages resulting from the use of any information, apparatus, method or process disclosed in this report.

As used above, "person acting on behalf of NASA" includes any employee or contractor of NASA, or employee of such contractor, to the extent that such employee or contractor of NASA, or employee of such contractor prepares, disseminates, or provides access to, any information pursuant to his employment or contract with NASA, or his employment with such contractor.

Requests for copies of this report
should be referred to:

National Aeronautics and Space Administration
Office of Scientific and Technical Information
Washington 25, D.C.
Attention: AFSS-A

CR-54245
GDA DBE 64-052-4

FINAL REPORT

DEVELOPMENT OF A COAXIAL PLASMA GUN FOR SPACE PROPULSION

by

Terence J. Gooding, Alan V. Larson,
Bruce R. Hayworth, and David E. T. F. Ashby

Space Science Laboratory

prepared for
NATIONAL AERONAUTICS AND SPACE ADMINISTRATION

April 1965

CONTRACT NAS 3-5759

Project Manager
NASA Lewis Research Center
Cleveland, Ohio
Spacecraft Technology Division
Mr. Peter Ramins

G E N E R A L D Y N A M I C S/C O N V A I R
S a n D i e g o, C a l i f o r n i a

TABLE OF CONTENTS

LIST OF FIGURES

LIST OF FIGURES

1.0 FOREWORD

This report is presented in partial fulfillment of contract NAS-3-5759; it contains a description of the work carried out during the fourth year of an experimental program to evaluate the pulsed coaxial plasma gun as a thrustor for space vehicles. The research of the first three years is summarized in the final reports of the previous contracts.[1,2,3]

2.0 INTRODUCTION

It is apparent now that pulsed plasma thrustors can be operated in two modes. In the first mode the current distribution moves and, acting like a piston, expells plasma. In the second mode plasma is accelerated by a stationary current distribution; in this case neutral gas or plasma moves into the current carrying region and is accelerated by magnetic and/or aerodynamic forces as in D. C. plasma thrustors. The concept of pulsing what are essentially D. C. accelerators was conceived and tested at this laboratory last year; the name Pulsed Arc Gun has been coined for this accelerator.

Conventional pulsed plasma guns, with moving current sheets, suffer from the disadvantage that the pulse-time is limited by the transit time of the current sheet along the electrodes. Typical periods are from 1 to 10 μsec, consequently low inductance energy storage capacitor banks are required and rapid propellant switching must be employed. For practical missions tens and possibly hundreds of millions of discharges are necessary and attaining adequate reliability may be

difficult. All of these problems are eased in the Pulsed Arc Gun; the period can be increased to 1 millisec without difficulty, the capacitor bank need not be closely coupled to the accelerator (a very desirable feature and mandatory for attitude control and station keeping applications), and slower gas switching can be used. Also, the efficiency should be higher than in conventional accelerators because magnetic energy is not being continuously fed to an expanding region behind a moving current sheet and there is no need to supply the large amounts of internal energy produced when a moving current sheet entrains and compresses the neutral gas ahead of it.[3]

The first three years of this program were devoted entirely to moving current sheet accelerators; during the past year, an increasing amount of effort has been spent investigating the Pulsed Arc Gun because of its potential advantages as a thrustor.

3.0 REVIEW OF PREVIOUS WORK

At the beginning of this program the coaxial gun was chosen because it is simple in concept, it offers the possibility of extreme reliability, and is a device in which the plasma is always tightly coupled to the magnetic field as distinct from inductive guns. The original design was based on the model of a current sheet accelerating a constant mass of gas;[1] a gun with a short barrel length and a correspondingly short electrical period was used in order to limit the time available for the growth of instabilities at the interface between the magnetic field and the plasma. It was considered that these constraints would also minimize the electrode erosion. The gun was operated in the gas-triggered mode

because the lifetime of high current switches is too short for practical missions, and because scaling laws indicated that an extremely low source inductance ($\sim 10^{-9}$ H) was necessary for efficient operation.

In the first year a major effort was spent in developing diagnostic methods to measure the electric and magnetic fields in the gun. Detailed measurements of B_θ and E_z were made from which the ion density and ion velocity distributions were deduced under the assumptions that the electrons were the main current carriers and that there was no radial plasma motion. The conclusion drawn from these measurements was that an ionization wave propagated in the accelerator, imparting some forward momentum to the ions but insufficient to cause significant mass accumulation in the current sheet. We now believe that the assumptions outlined above are not valid, that ion current is important, and that the plasma is either brought to the velocity of the current sheet, or driven into the electrodes.

At the beginning of the second year a change in the gas distribution in the accelerator caused an instability in the current sheet. The current distribution, which was initially azimuthally symmetric, collapsed into a localized spoke. Later in the year we found that this instability could be avoided by injecting propellant uniformly into the interelectrode region.[4] However, in recent experiments with a gun in which the gas distribution was localized the instability did not occur.

During the second and third contractual periods the energy storage capacitance was increased, while the parasitic inductance was decreased, in order to improve the energy transfer to the accelerator.

By the end of the second year 65% of the initial stored energy could be delivered to the accelerator and the thermal efficiency was 25%.

During the third year, a capacitor development porgram was started to reduce the size, weight, and cost of the capacitor, while at the same time doubling the capacitance. In the course of this work a lightweight, low loss, low impedance distributed parameter pulse-line was developed.[3] Using this pulse-line an accurate energy inventory was made; it showed that ohmic losses were small, that 88% of the stored energy could be transferred to the accelerator and that this was shared approximately equally between work done on the current sheet and magnetic field energy, as expected. The maximum calorimetric efficiency obtained was 45% at an exhaust velocity of about 7 cm/μsec.

Toward the end of the third year a theoretical analysis of the energy loss mechanisms was made. It showed that about one-half of the work done on the current sheet appeared as internal energy in the plasma (because the current sheet was moving at a constant velocity into a gas of uniform density) and that this energy would be lost in radiation in a time comparable to the acceleration period.[3] Consequently the efficiency of the device, when operated in this mode, could not be greater than about 50%. This conclusion was borne out by the experimental observation that the maximum thermal efficiency was 45% for a wide range of operating conditions.

Two methods to overcome this limitation were proposed; in the one scheme the propellant was to be entrained in the current sheet at the beginning of the acceleration cycle and then accelerated through

vacuum; in the other scheme the plasma was to be accelerated by a stationary current sheet as in steady-state accelerators.

4.0 EXPERIMENTS

4.1 Moving Current Sheet Accelerators

4.1.0 Discussion

Coaxial guns with moving current sheets can be operated in two modes; the propellant is either picked up continuously by the current sheet (the snow-plow and shock models) or entrained initially and thereafter accelerated by it (the slug model). In some accelerators the current sheet reaches the end of the electrodes before the capacitor has completely discharged; in this situation the discharge may 'hang up' at the end of the accelerator and behave in a manner analogous to the Pulsed Arc Gun or it may continue to propagate and plume out into the vacuum chamber. One frequently finds that the thermal efficiency of the device is maximized if most of the stored energy is delivered after the plasma reaches the end of the electrodes. This mode is acceptable providing the thrust efficiency is also high. However, there are several effects that can occur in this mode that lead to erroneous measurements; the most common are phenomena associated with currents that flow from the accelerator to the walls of the vacuum tank, entrainment of neutral gas from the vacuum tank, and adsorption of propellant on the electrodes. In our experiments we always insure that tank currents are not present and we maintain a low ambient pressure $\sim 10^{-6}$ Torr to avoid the entrainment problem.

4.1.1 Switched Gun Experiments

The objective in these experiments was to study the dynamics of a current sheet moving into neutral gas of known density. High voltage switching was employed so that the electrodes and the vacuum chamber could be uniformly filled to the desired pressure before the discharge was initiated. The system was pumped out after each shot then refilled with the test gas.

Figure 1 is a diagram of the switched gun. The switch consists of two electrodes separated by a 1 mm gap pressured with dry air to 65 p.s.i. The gap breaks down and the switch becomes conductive when the gap pressure is reduced by opening an electrically operated tap. The only difficulty incurred was in making the inductance low enough so that the discharge current could build up in a time short compared with the pulse-time. The lowest inductance obtained was approximately 6 nH of which about 5 nH was in the spark. The gun was connected to a pulse-line with an impedance of 17 m Ω and a pulse-time of 0.8 μsec.

The magnetic and electric fields associated with the current sheet were measured for nitrogen at three different densities (100, 200, and 400 m Torr). The behavior of the current sheet was essentially the same as observed before in a gas-triggered gun. Figure 2 shows oscillograms of B_θ at different axial positions and Figure 3 the corresponding profiles of B_θ; in this case the filling pressure was 200 m Torr and the pulse-line was charged to 4.5 kV. The inner electrode was always negative and at each filling pressure a current sheet 1 to 2 cm thick formed which carried 80% or more of the current; the radial electric field behind the

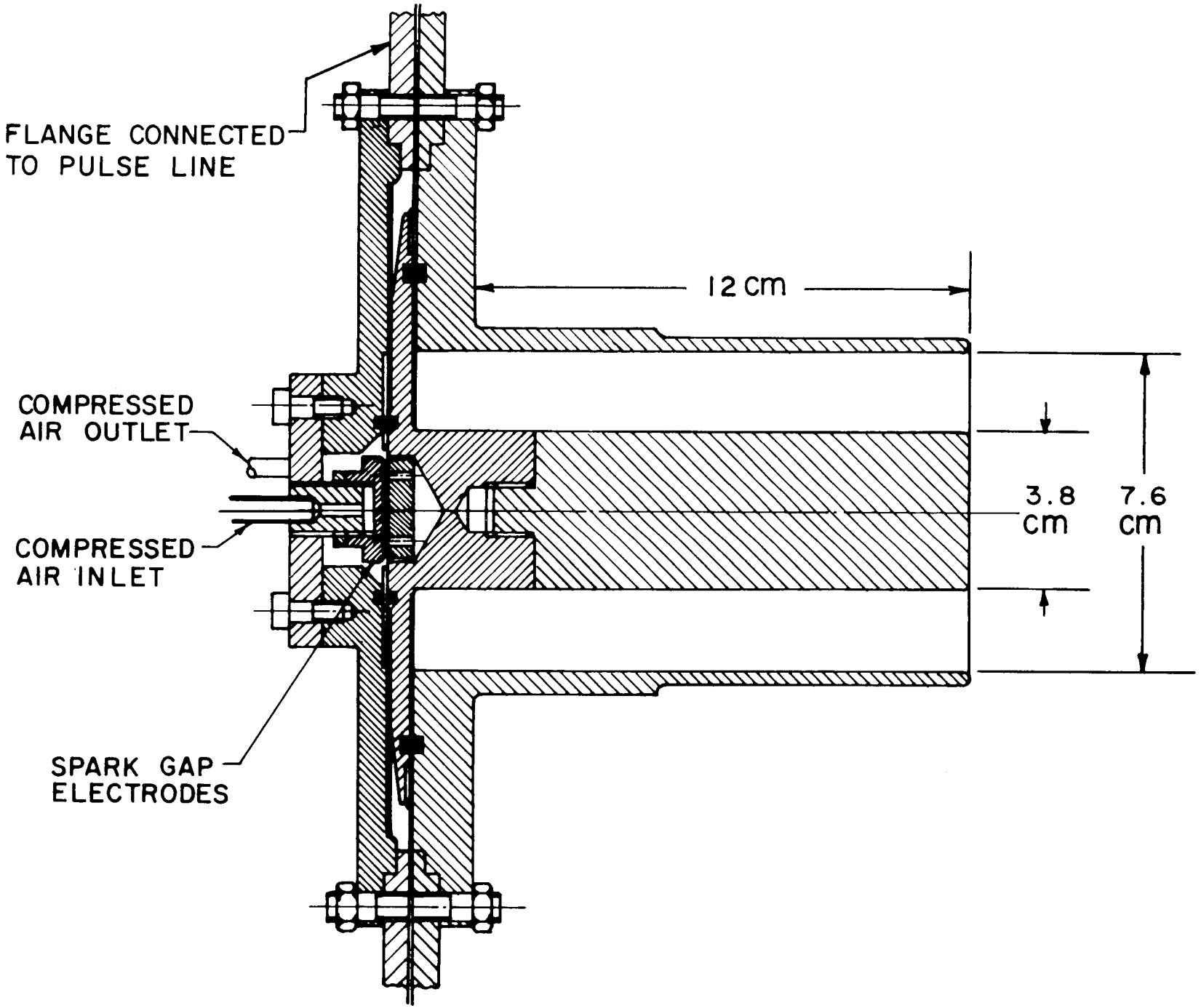

FIG. 1 : SWITCHED COAXIAL GUN

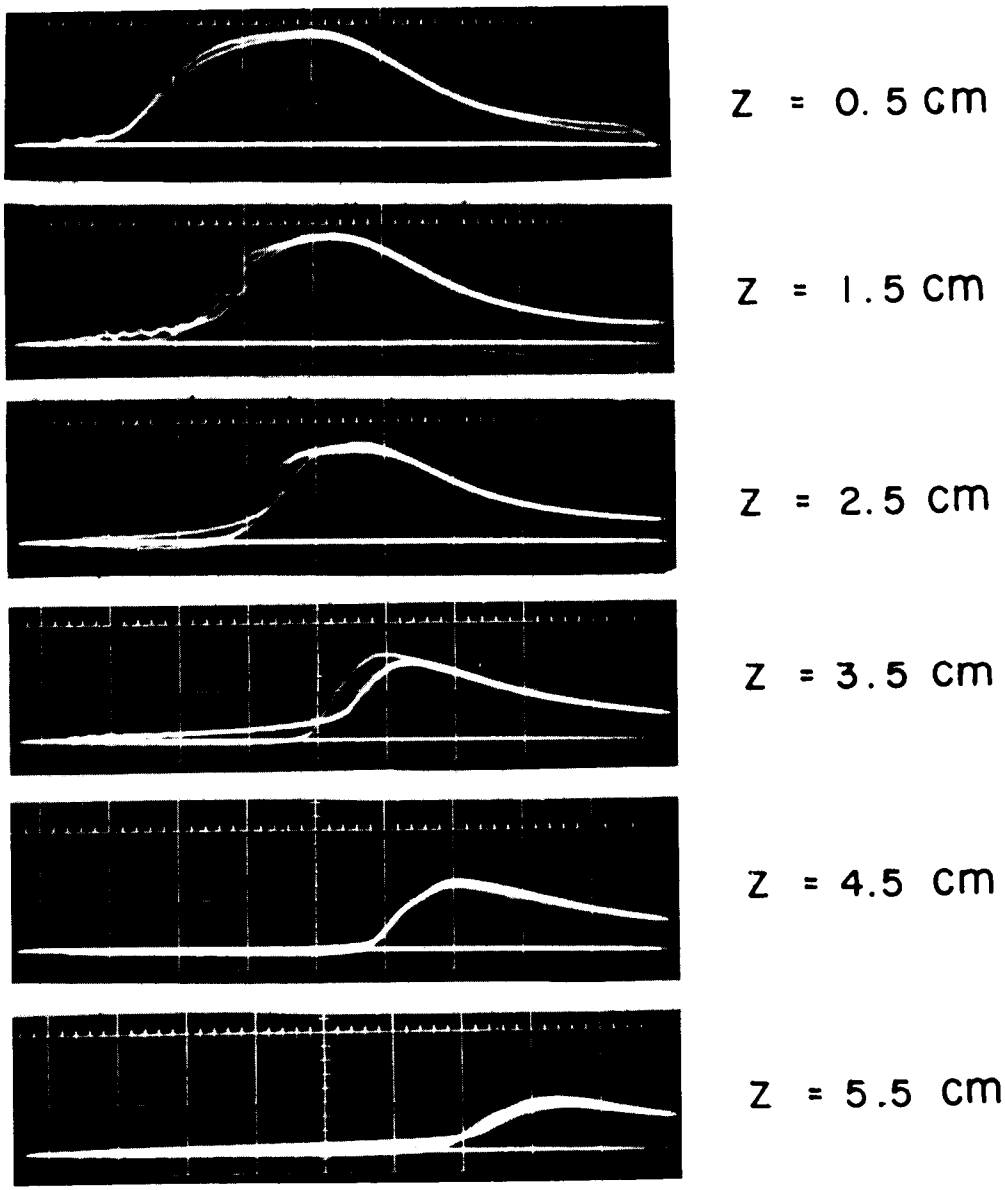

FIG. 2 : OSCILLOGRAMS OF B_θ , z = AXIAL POSITION,
B_θ = 5.4 kG/cm , t = 0.2 μsec /cm ,
p = 200 m TORR NITROGEN

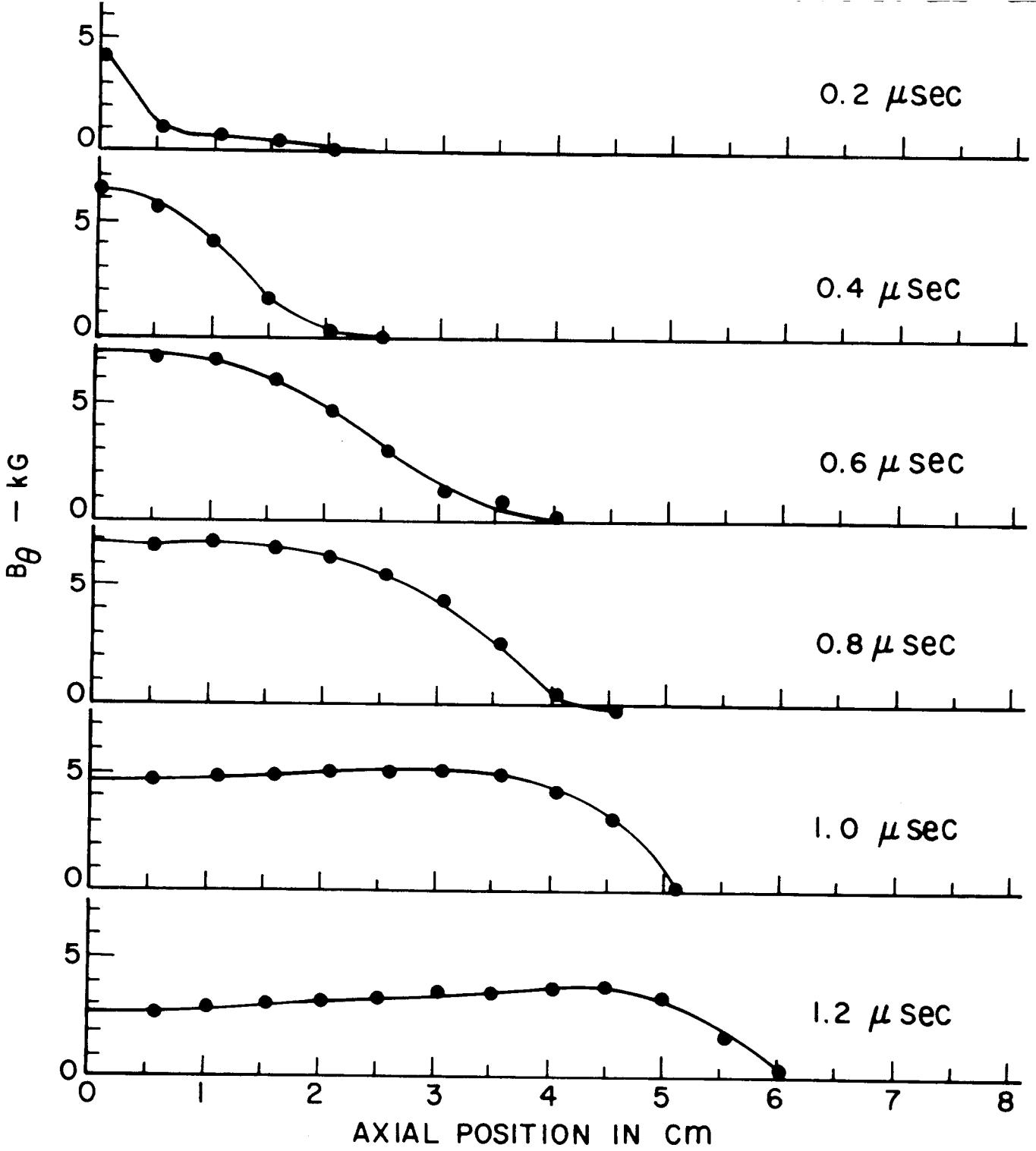

FIG. 3 : AXIAL DISTRIBUTIONS OF B_θ . p = 200 m TORR NITROGEN

sheet was equal to $\bar{B}_\theta \times \bar{v}_s$ to within experimental error. (v_s is the measured sheet speed.) These two facts argue strongly that there can be little plasma behind the current sheet and that the neutral gas that it sweeps up must be either retained or driven into the electrodes.

If it is assumed that the current sheet acts as a perfect snow-plow and does not lose mass, then its position can be calculated as follows:

$$\frac{B^2}{2\mu_o} = \frac{d}{dt}(Mv) \tag{1}$$

$$\therefore \int_o^t B^2 dt = 2\mu_o Mv = 2\mu_o \rho z \, dz/dt \tag{2}$$

$$\therefore \int_o^t \int_o^t B^2 \, dt \, dt = \mu_o \rho z^2 \tag{3}$$

$$\therefore \int_o^t \int_o^t I^2 \, dt \, dt = (M'/L') z^2 \tag{4}$$

where I = total current

M' = initial mass of gas per unit length of barrel

L' = inductance per unit length of barrel

z = axial position of the current sheet

ρ = neutral gas density

The double integral in Equation (4) can be evaluated from the measured gun current and then used to predict the position of the current sheet on the assumption that the current sheet retains all the mass it encounters.

The calculated sheet position agrees very well with the measurements (see Figure 4) providing the value of B at the inner electrode is used in Equation (3). This result is in agreement with the theory given by Fishman and Petschek[5] or indeed any theory that assumes that the current sheet is normal with the center electrode.

The main conclusion drawn from these experiments was that, for practical purposes, the simple snow-plow model is adequate for explaining the dynamics of current sheets in coaxial guns operating at currents $\sim$ 100 kA, and particle densities $\sim 10^{15}$ to 10^{16}/cc when the interelectrode region is uniformly filled with gas.

4.1.2 Gas-Triggered Gun Experiments

4.1.2.1 Uniform Mass Loading

The objective in these experiments was to determine the dependence of the current sheet velocity, the exhaust velocity, and the calorimetric efficiency on the gun voltage, current, and dimensions, in a gas-triggered gun uniformly filled with propellant. These experiments follow-up those described in the previous section; however, it is difficult to make a direct comparison between theory and experiment in this case because of uncertainties in the absolute value of the neutral gas density.

The gun is shown schematically in Figure 5; the propellant is injected through several sets of gas ports spaced uniformly along the electrodes. Several pulse-lines, with different impedances and pulse-times were used; the method of construction of these lines is described in Reference 3.

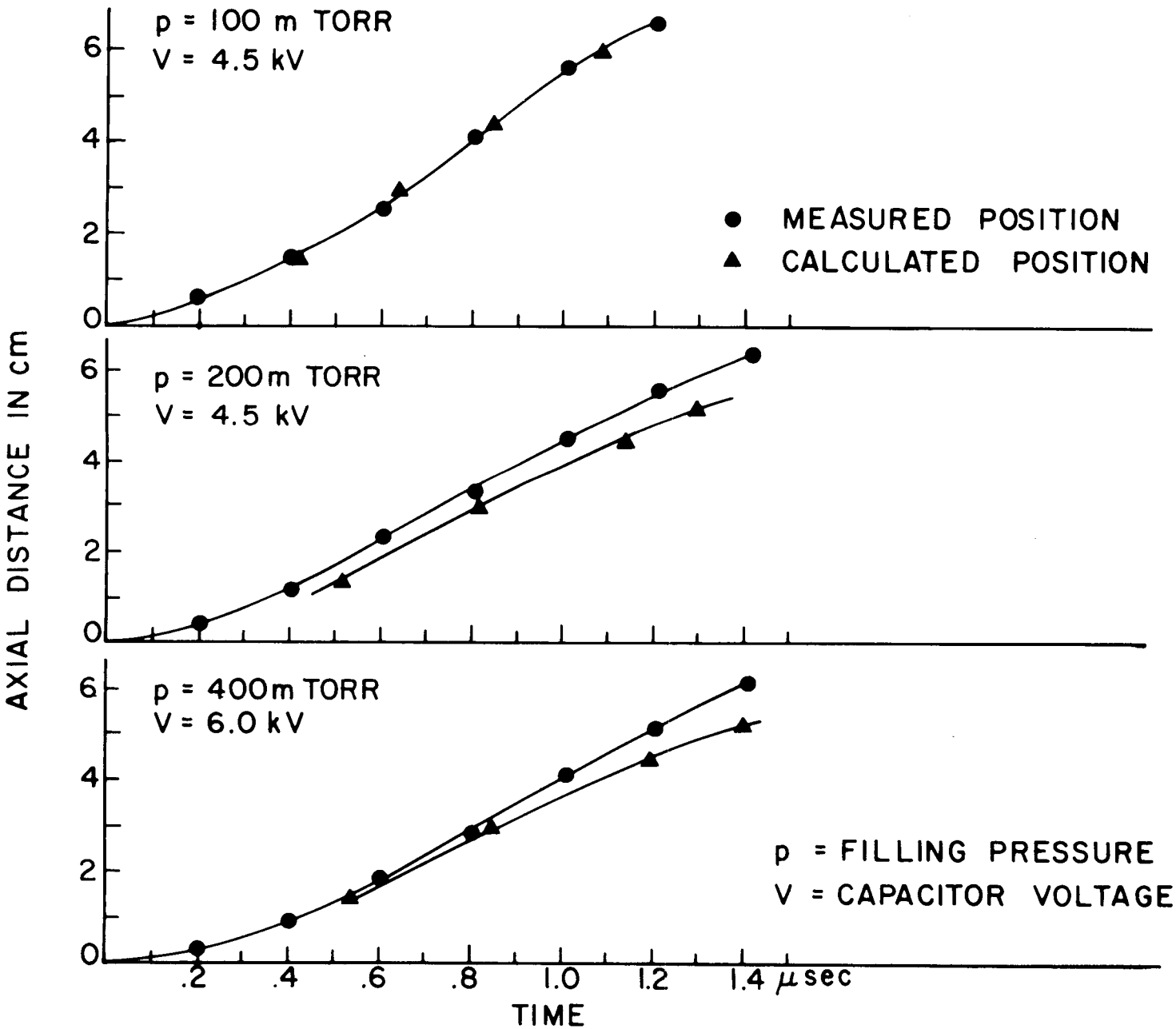

FIG. 4 : CURRENT SHEET POSITION IN THE SWITCHED GUN. UNIFORM GAS FILL.

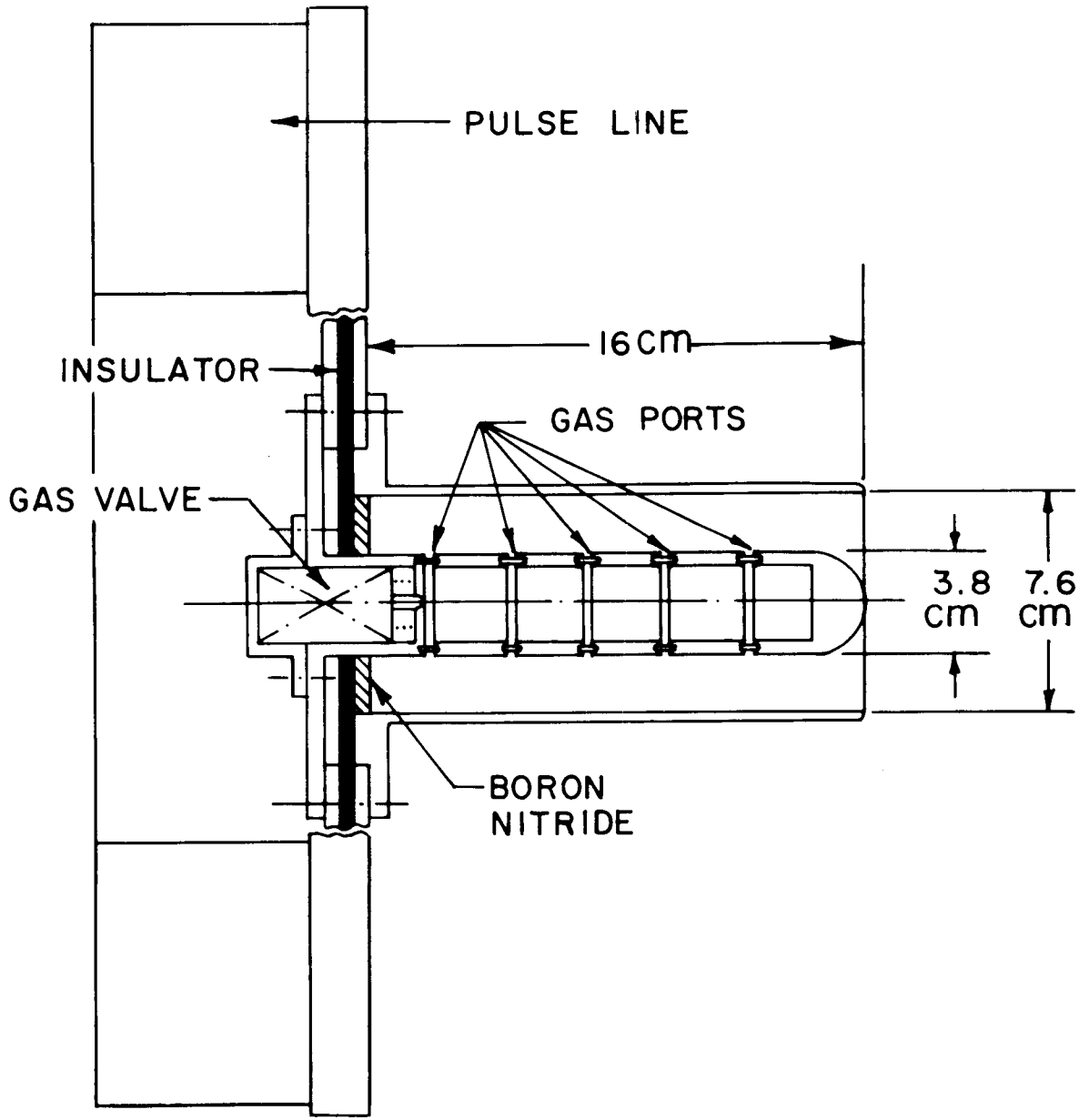

FIG. 5 : SCHEMATIC DIAGRAM OF THE GAS TRIGGERED GUN.

Typical oscillograms of voltage and current are shown in Figure 6, together with magnetic probe data taken with two probes placed symmetrically on opposite sides of the barrel and at mid-radius. Superimposed are B_θ values observed by the probes when placed at 0, 2, 4, 6, and 8 cm from the insulator. In this case the barrels were 10 cm long and it is seen that the current sheet reaches the muzzle as the current begins to decrease.

The current sheet velocity can be determined from the magnetic probe data or by observing the magnitude of the first step on the voltage waveform. The latter technique is possible because the current reaches its terminal velocity in a few tenths of a microsecond and propagates at constant velocity for the duration of the pulse. When $\dot{I} \sim 0$ the following equation applies:

$$\frac{V_B}{V_o} = \frac{L' v}{L' v + Z_L} \tag{5}$$

Where V_o = applied voltage, V_B = breech voltage, L' = inductance per unit length of the electrodes, v = current sheet velocity, and Z_L = line impedance. Velocities calculated using Equation (5) are typically within 15% of the velocities determined by B_θ probes.

The experiments described in the previous sections suggest that the simple snow-plow model can be used to determine the functional dependence of v. The momentum equation

$$\frac{B^2}{2\mu_o} = \frac{d}{dt}(Mv) = \dot{M}v + M\dot{v} \tag{6}$$

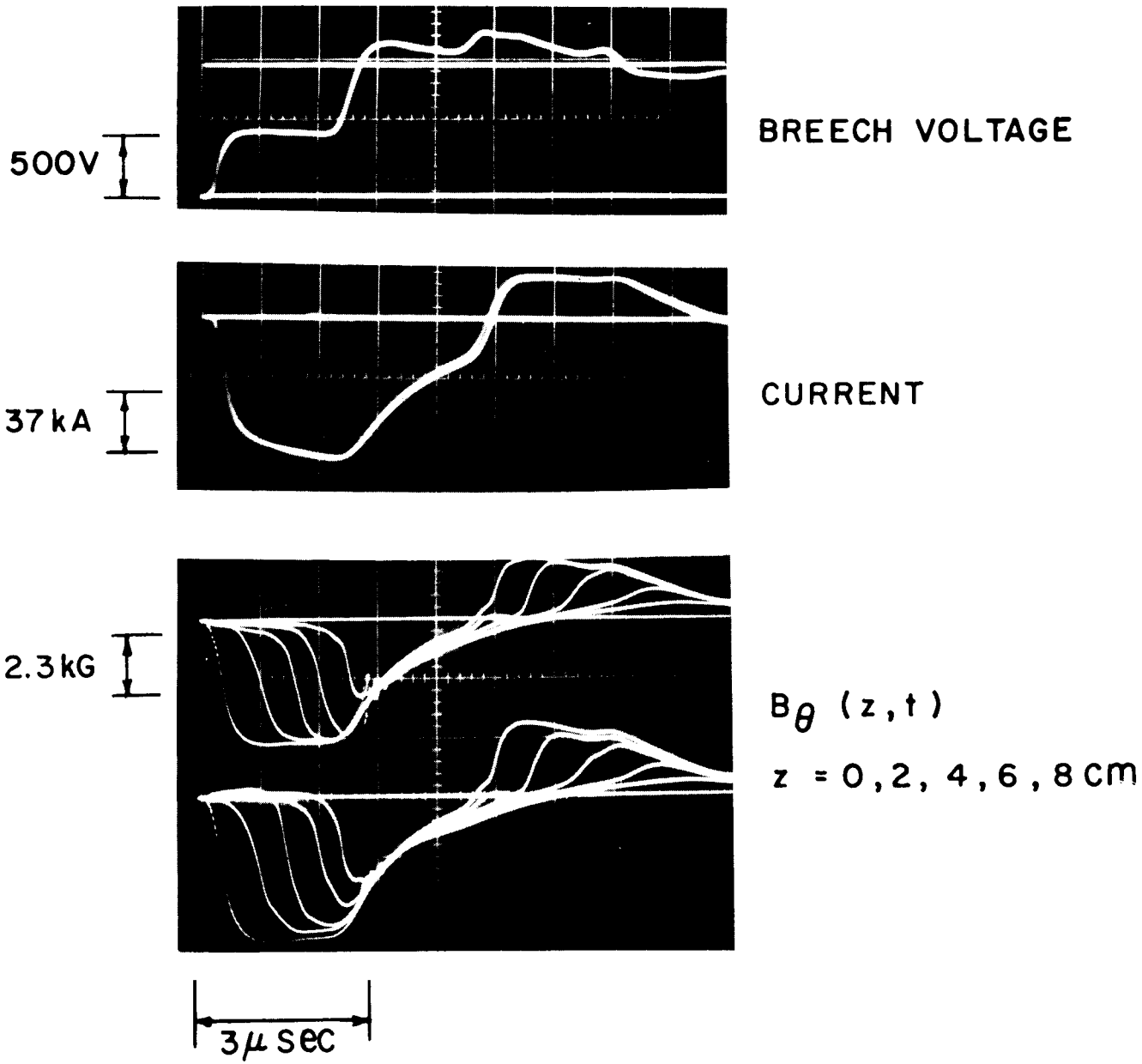

FIG. 6 : OSCILLOGRAMS OF VOLTAGE, CURRENT AND $B_\theta(z,t)$
5.6 m Ω PULSE LINE, NITROGEN PROPELLANT.

and the experimental observation that $v \sim \frac{E}{B}$, $\dot{v} \sim 0$, and $\dot{I} \sim 0$ for most of the discharge period leads to the relationship

$$v = \left(\frac{L'}{2\rho A}\right)^{1/2} I \; ; \qquad (7)$$

where the mass density ρ is assumed uniform, A is the cross-sectional area of the interelectrode space and I is the total current.
The current sheet velocity was measured as a function of current for H_2, N_2, and Xe propellants; the data shown in Figure 7 was obtained with a gun which was 10.3 cm in length and connected to a pulse-line with an impedance of 17 m Ω and pulse-time of 0.8 μsec. The sheet speed is approximately proportional to current, as predicted by Equation (7). In these measurements gun current was varied by changing the gun voltage, consequently the neutral gas density was not constant. However, the neutral gas density changed by less than a factor of 1.5 over the voltage range used and since the sheet speed depends on $\rho^{-1/2}$, it was hardly affected by this change. A typical neutral density profile, measured with a fast ionization gauge[3] is shown in Figure 8; the errors are relative with an absolute error of $\pm$ 50%. The measured sheet speeds agree with the values predicted by Equation (7) within this accuracy.

The exhaust velocity and calorimetric efficiency depend on the matching between the accelerator length, the sheet velocity, and the pulse-time. Oscillograms taken with a negatively-biased Faraday-Cup ion probe situated 140 cm from the gun are shown in Figure 9 for three

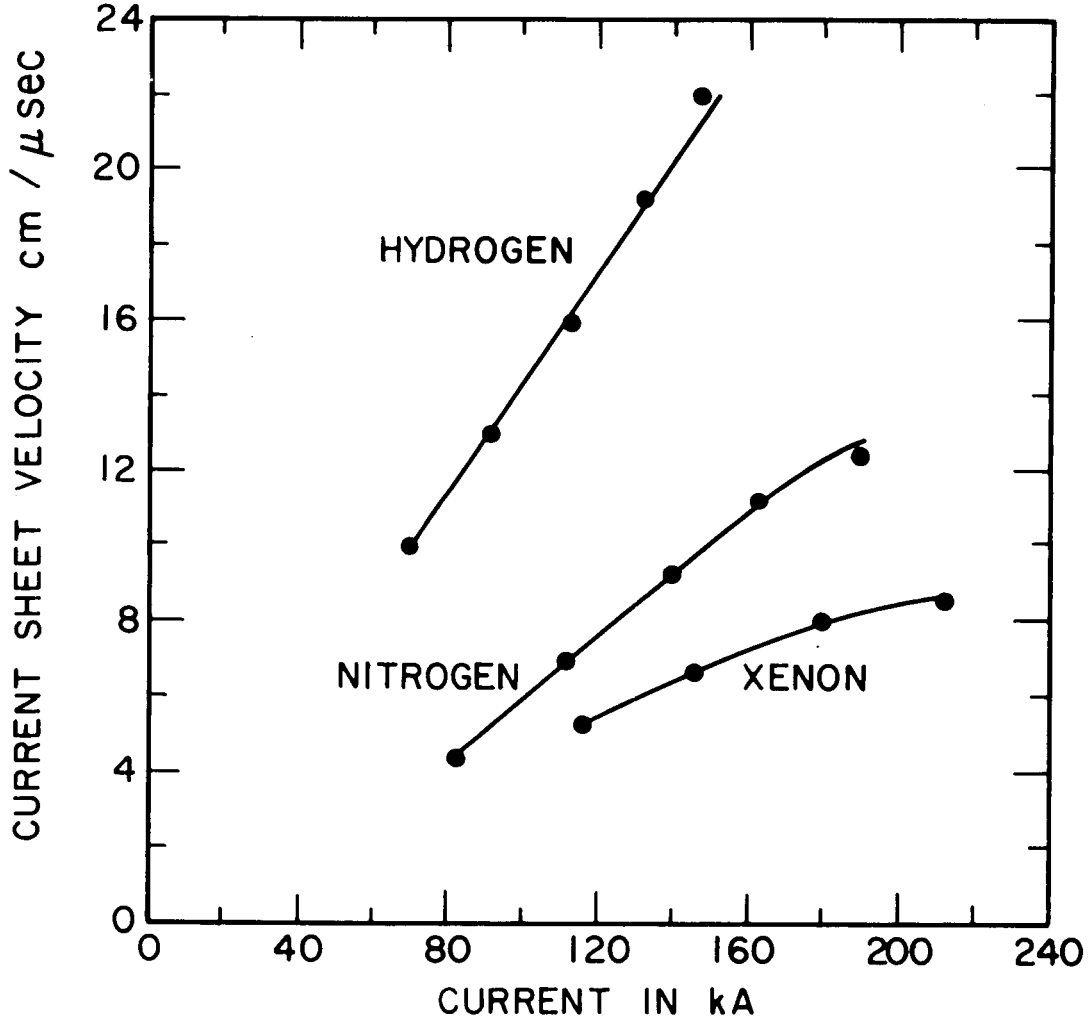

FIG. 7 : VARIATION OF CURRENT SHEET VELOCITY WITH CURRENT

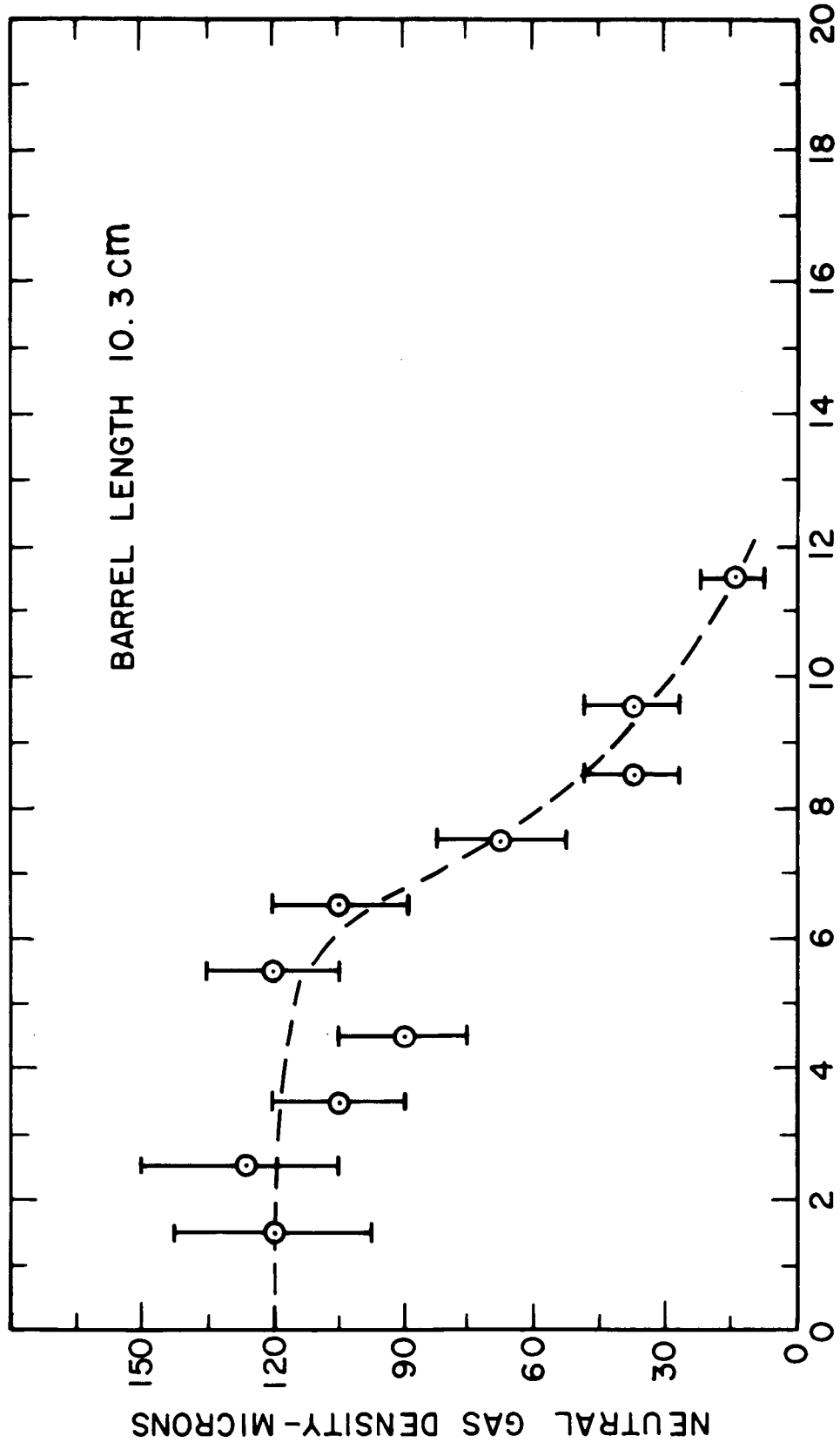

FIG. 8 : NEUTRAL GAS DENSITY PROFILE

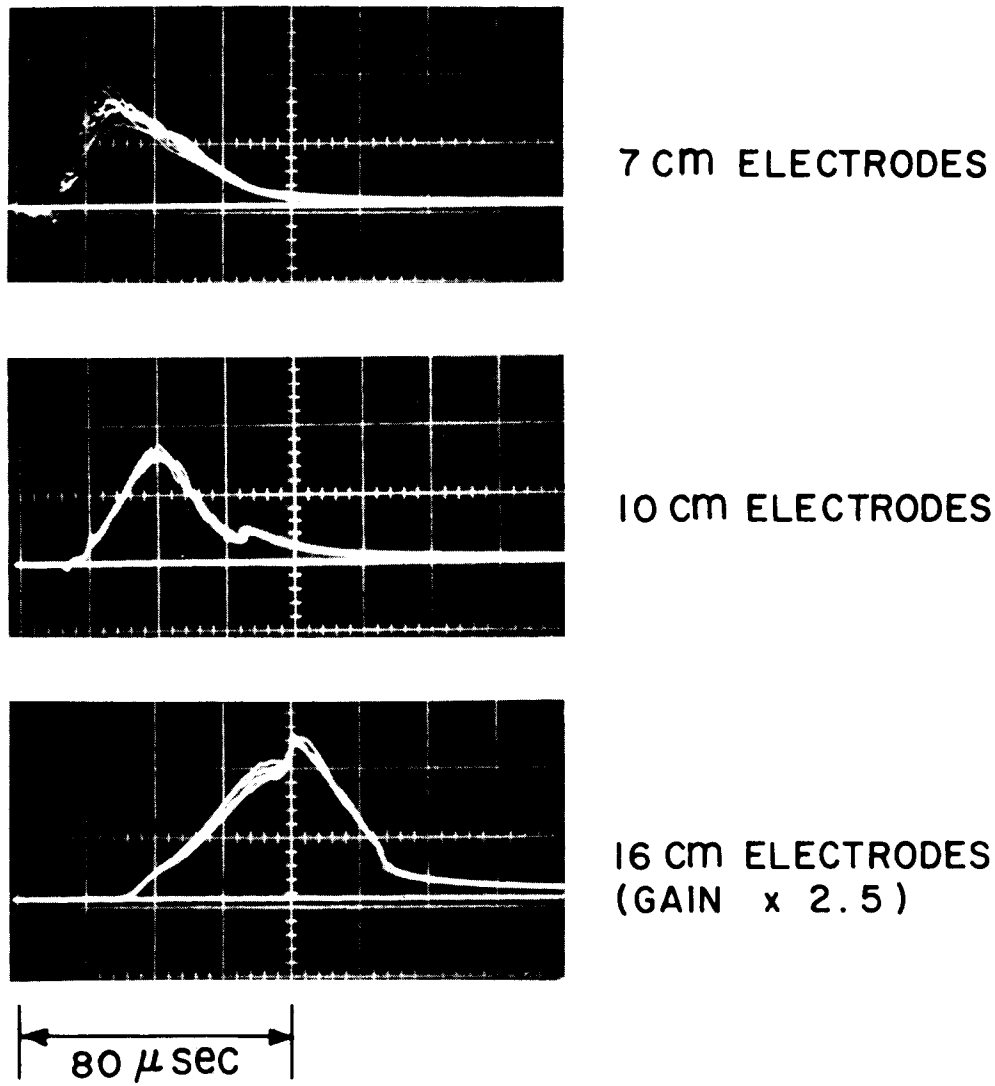

FIG. 9 : ION PROBE OSCILLOGRAMS, 140 cm FROM THE GUN

electrode lengths, 7 cm, 10 cm, and 16 cm. This data was taken with the electrode arrangement shown in Figure 6 and a pulse-line of 5.6 m Ω impedance and 2.2 μsec pulse-time. The gun voltage was 1100 volts and the current was 80 kA; the current sheet velocity was 3.9 cm/μsec. The average exhaust velocity is approximately equal to the sheet speed if the current sheet reaches the muzzle just before the current starts to decay. This behavior was common to all of the accelerators investigated. It should be noted that if the current just starts to decay as the current sheet reaches the muzzle then at this time the magnetic field energy within the accelerator is about equal to the work done on the current sheet and that this field energy must be recovered in order to have efficient operation!

The main conclusions from these experiments were that the current sheet dynamics agree with a simple snow-plow model, the plasma emerges at the current sheet velocity if it is driven to the ends of the electrodes and that the thermal efficiency is maximized at about 45% when the current pulse ends as the current sheet reaches the muzzle.

4.1.2.2 Non-Uniform Mass Loading

The primary objective of these experiments is to make a mass-loaded current sheet accelerate continuously and thereby reduce the energy expended in internal energy. This objective can be met in principle by employing a gas distribution which is peaked at the breech of the accelerator. The practical difficulties involved relate to obtaining the desired gas distribution, maintaining azimuthal symmetry in the current sheet and recovering the magnetic field energy behind

the current sheet.

So far we have not obtained significant acceleration of a current sheet. The most severe problem is getting the appropriate gas distribution at a high enough density so that the current can be drawn from the plasma without seriously depleting the total mass. At first, we tried to employ gas triggering and adjust the gas distribution by the arrangement of the gas ports; this method was not satisfactory so a high voltage switch was added to the gun. At the same time a fast-acting gas valve was installed. This system is being studied now.

Several experiments were performed using a gas-triggered gun with a single set of gas ports near the breech. The current sheet propagated much the same as in the uniform fill experiments until it approached the region where the gas density dropped. At this point the leading edge of current sheet accelerated while the central portion did not.

In another experiment the pulse-time was extended to about 10 μsec by using a low impedance pulse-line and electrodes with a large radius ratio. In this case the load impedance was large compared to the line impedance, and several voltage reflections in the line occurred before the breech voltage reversed. Axial gas injection was employed. The current sheet formed at the breech of the gun, propagated along the barrels in the same manner as in the uniform fill experiments, then continued past the muzzle of the gun and plumed out into the vacuum chamber. Most of the energy was delivered to the plasma when the current

sheet was past the muzzle. These experiments were done in a small vacuum chamber which unfortunately was not instrumented to measure thermal efficiency.

In some of these experiments we found that up to 50% of the total current was returning via the vacuum tank walls. These currents were eliminated by 'floating' the gun and gas valve assembly.

4.2 Stationary Current Sheet Accelerators

4.2.1 Pulsed Arc Gun with Cylindrical Electrodes

The initial experiments on the Pulsed Arc Gun were done with a gun with a 3-inch diameter outer electrode and a 1.5-inch diameter inner electrode. The gun used is shown in Figure 10. It was connected to a lumped parameter pulse-line made from 240 μF capacitors; the pulse-line typically consisted of 5 sections and had an impedance of $\sim$ 100 m Ω and a pulse-time of $\sim$ 150 μsec. The line was always charged to less than 1 kV. The gun was gas-triggered by the propellant gas which was pulsed through twelve 3/8-inch holes in the insulator at the back of the gun. In order to encourage rapid breakdown at low gas density the gas initially entering the barrels was weakly ionized by a gas-triggered discharge between the ignitor, shown in Figure 10 and the main electrodes. Both nitrogen and hydrogen propellants were used with this gun.

Figure 11 shows oscillograms of gun current and voltage and ion probe output. The noise in the voltage trace is characteristic of the gun and is also present on B_θ signals, measured with magnetic probes. The probe signals show that the magnetic field has gross azimuthal symmetry and that the current density is uniformly distributed between

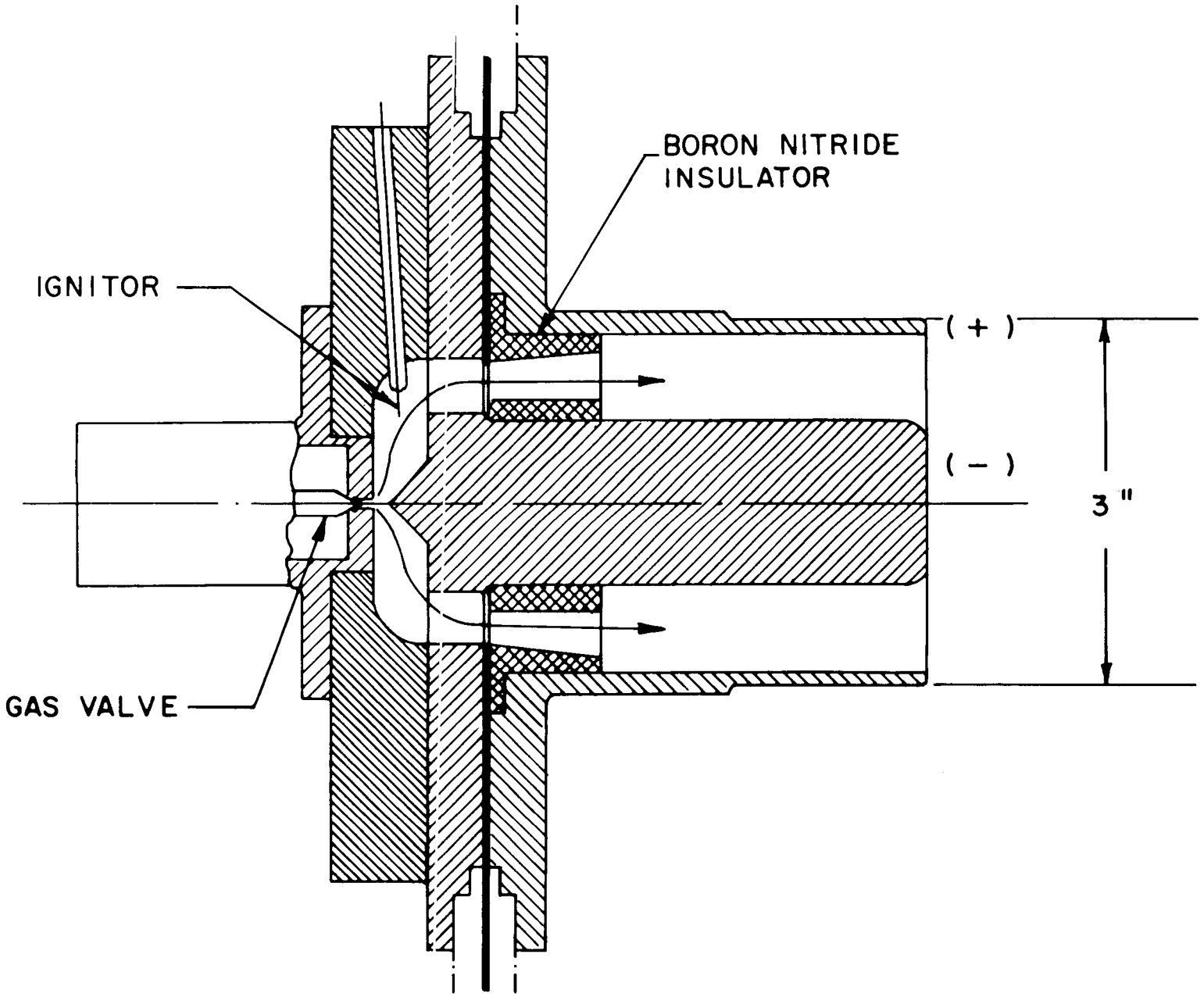

FIG. 10 : PULSED ARC GUN, WITHOUT EXTERNAL MAGNETIC FIELD.

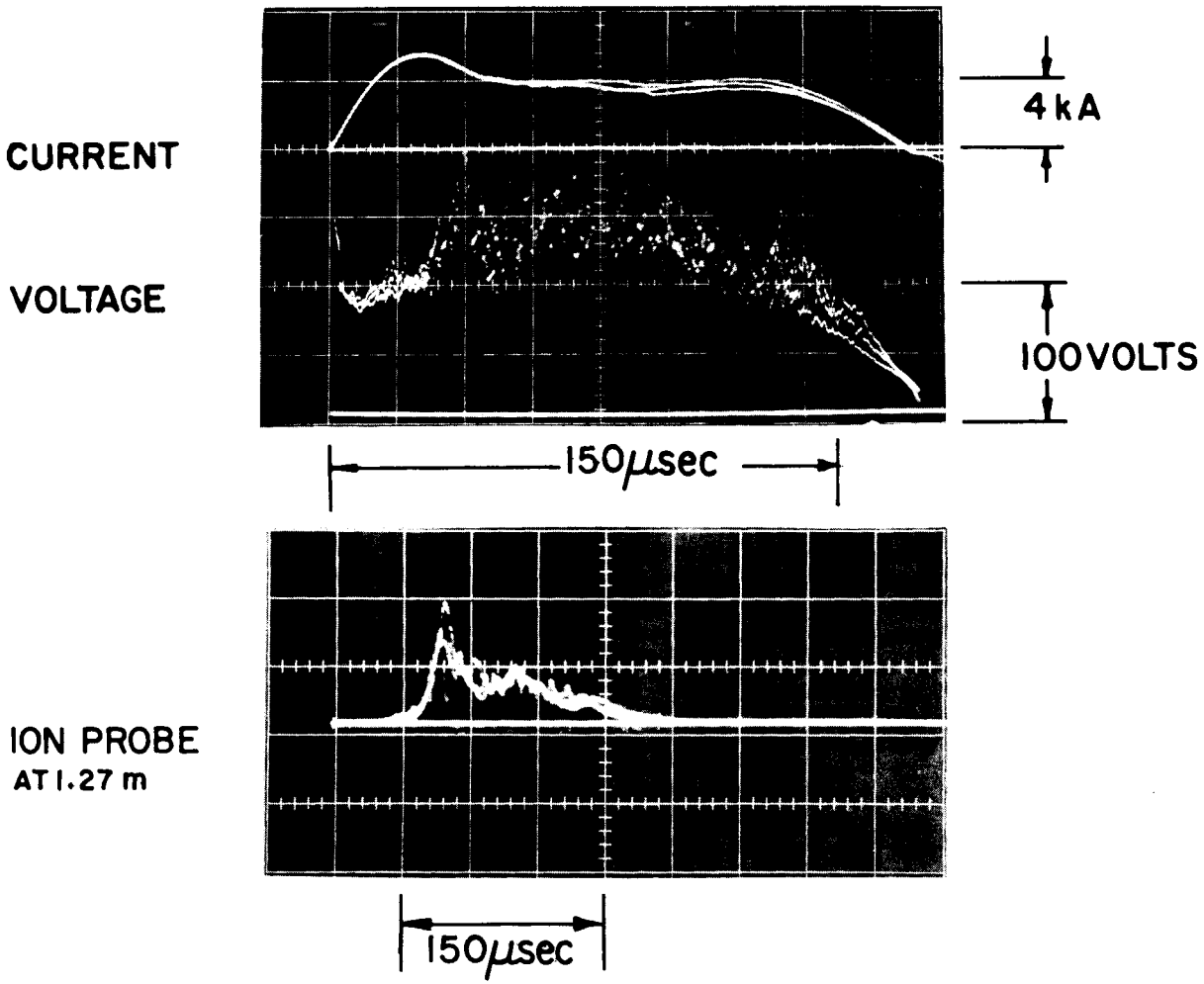

FIG. 11 : OSCILLOGRAMS FOR PULSED ARC GUN WITHOUT AN EXTERNAL MAGNETIC FIELD, NITROGEN PROPELLANT

the electrodes with little current flowing past the end of the center electrode.

Experiments with the Pulsed Arc Gun are complicated by a tendency for current to flow from one electrode to the vacuum tank and then to return to the other electrode via the tank walls. This current is evidenced by arc-spots on the walls and is measured by a Rogowski belt around the conductor which connects the ground electrode of the gun to the tank. Up to 50% of the total gun current has been observed to flow to the tank walls. Electrically isolating the gun from the tank offers no solution because, in this case, a discharge tends to occur across the isolating insulator between the gun and the tank; if breakdown occurs at this insulator tank current flows but it is difficult to measure. Insulating the entire end flange does not appear worthwhile because arc-spots often appear on the side walls and it is impractical to insulate the entire tank. Tank currents generally occur when the gun voltage exceeds 150 volts; because lower voltages should be adequate for producing plasma velocities of 1 - 5 x 10^6 cm/sec the operation of the gun has been restricted to voltages where the tank currents do not flow.

Figure 12 shows oscillograms of the output from an ion energy analyzer (see Appendix I-1) used to measure ion energies in the exhaust. The exhaust velocity, determined by time-of-flight between the ion probe and the energy analyzer is $\sim$ 3-4 cm/μsec in the case illustrated. The energy analyzer shows that the ion energy is greater than 70 eV and that some doubly ionized ions are probably present during the acceleration process.

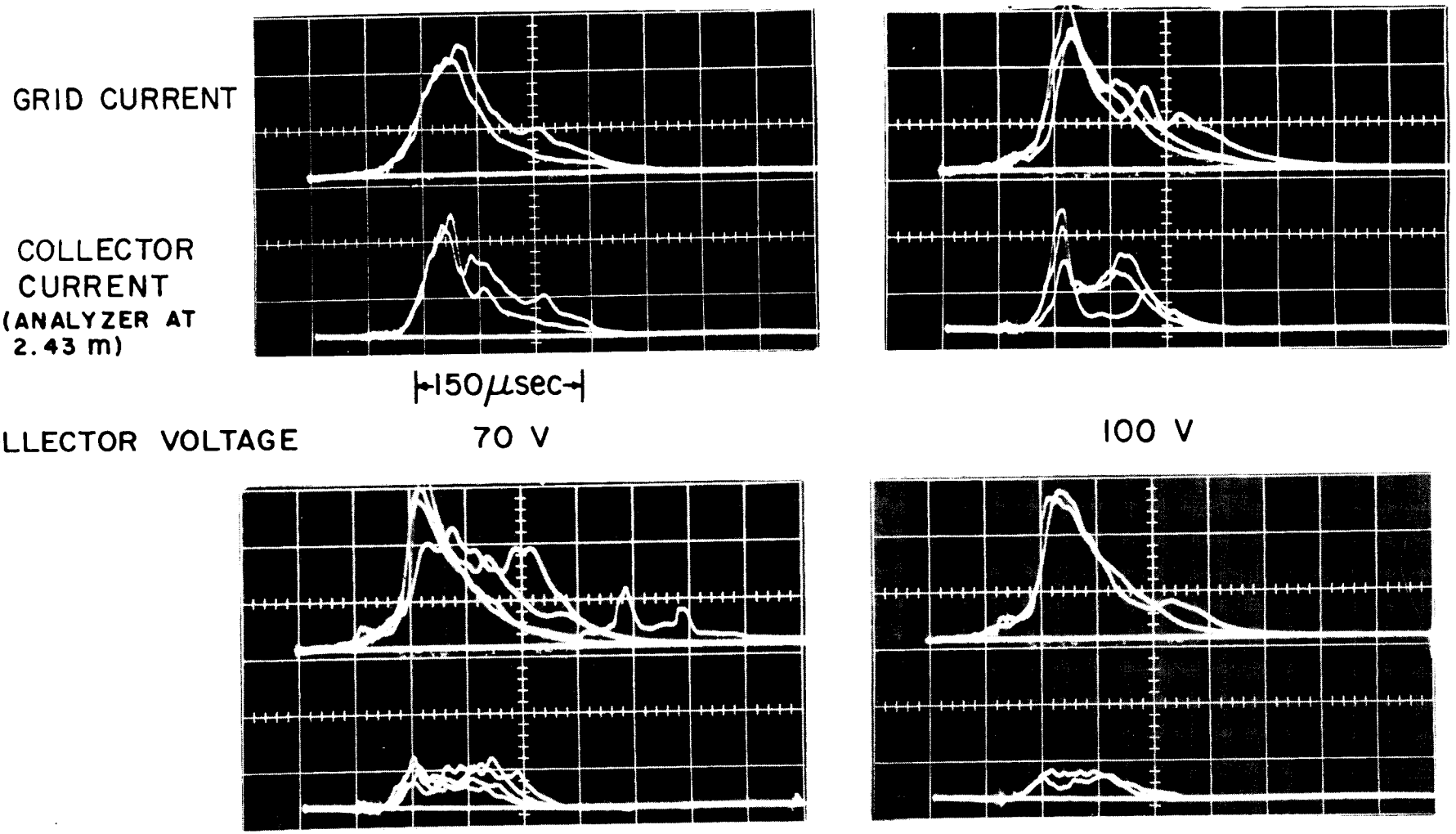

FIG. 12 : ION ENERGY ANALYZER OSCILLOGRAMS, NITROGEN PROPELLANT

The use of ion probes and particle analyzers is complicated by the fact that the exhaust plasma leaves the gun with an electrostatic potential close to the cathode potential. Figure 13 illustrates this behavior. The two pairs of oscillograms compare the terminal voltage with the plasma potential measured by a floating probe 260 cm downstream. In both cases the center electrode is the cathode during the first half-cycle while the outer electrode becomes the cathode after voltage reversal. However, in the first case the outer electrode is at ground potential while in the second case the center electrode is grounded. In order to avoid high plasma potentials the gun is normally operated with the center electrode, which is the cathode, at ground potential. However, as can be seen from Figure 13, the plasma still acquires a potential of approximately 100 V during the second half-cycle and a bias voltage in excess of this must be applied to an ion probe if it is to function properly after voltage reversal.

Measurements of calorimetric efficiency show that typically about 15% of the electrical energy supplied to the terminals of the gun appears in the exhaust. Higher efficiencies are measured if the gun voltage is increased and tank currents are allowed to flow!

To clarify experimentally the difference between the Pulsed Arc Gun and the conventional coaxial gun the barrel length was increased from 7 cm to 25 cm. The object of this change was to see if the current distribution could be held near the breech insulator, by continually feeding it with gas, or whether it would always move to the end of the electrodes. In every case the discharge reached the end of the electrodes; however, two distinct modes of operation were observed. The first occurred

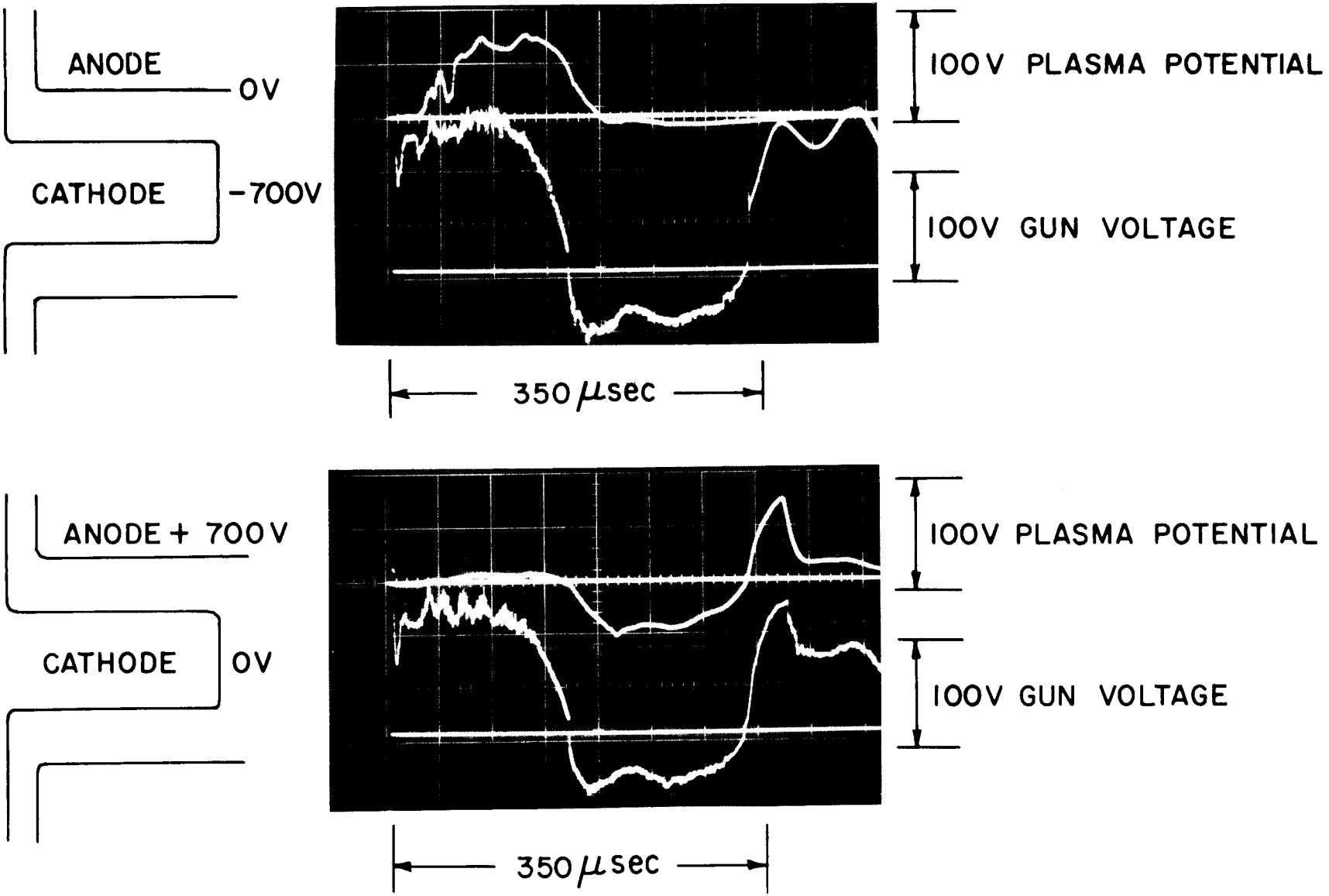

FIG. 13 : OSCILLOGRAMS DEMONSTRATING THE RELATIONSHIP BETWEEN CATHODE AND PLASMA POTENTIALS (2.43m DOWNSTREAM, UPPER OSCILLOGRAM INVERTED)

if the ignitor was not used; in this case breakdown was delayed and the barrels filled with gas before firing. In the second case breakdown occurred as soon as gas entered the barrels which consequently were essentially empty at breakdown. The neutral density distribution was determined with a fast ionization gauge.

With gas-filled barrels magnetic probe measurements showed that a distinct current sheet propagated along the barrels; when the sheet reached the muzzle it slowly thickened until current was flowing throughout the interelectrode space and within 5-10 cm of the breech insulator. With empty barrels the interelectrode space rapidly filled with diffuse current but without a precursor current sheet. Figure 14 shows profiles of B_θ and compares the two cases.

To investigate the current flow further a small Rogowski probe was made which measured the local value of j_r; this probe confirmed the results obtained with the B_θ probes but showed dramatically that the current density was non-uniform and that the current was apparently carried in numerous filaments. Figure 15 shows oscillograms obtained with the Rogowski probe at different positions along the length of the barrels; each oscillogram consists of several traces overlaid. If the height of the smaller spikes corresponds to a single filament of current threading the Rogowski then each filament carries about 200 amp; this figure is typical of arc-spots and it is concluded that the electron current is produced predominantly by arc-spots.

Figure 16 is a space-time plot showing the position of the current sheet, for the case of gas-filled barrels, and also the position of the plasma front ejected from the gun. It can be seen that a short time after the current sheet reaches the end of the barrel plasma is

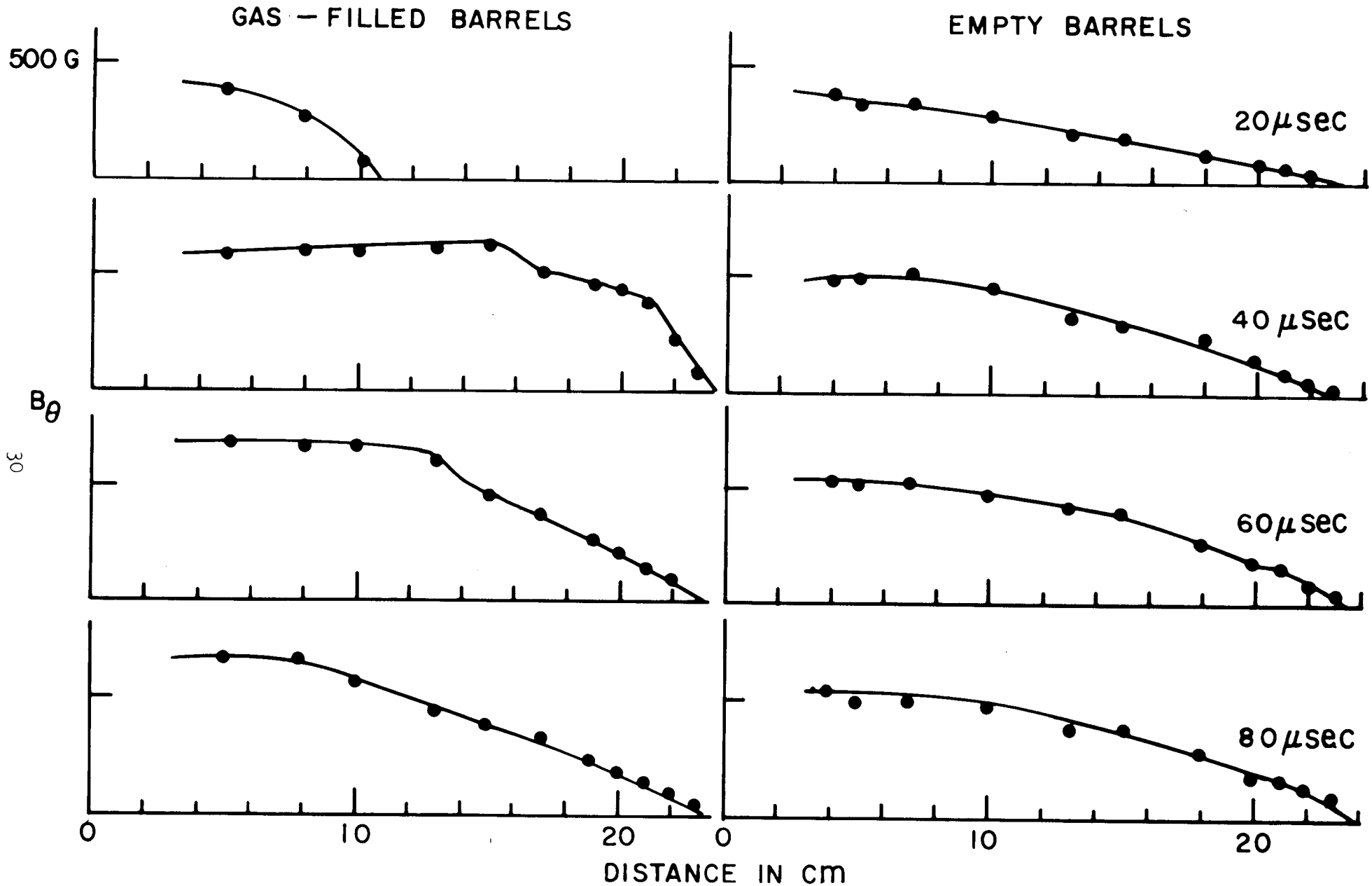

FIG. 14 : B_θ PROFILES

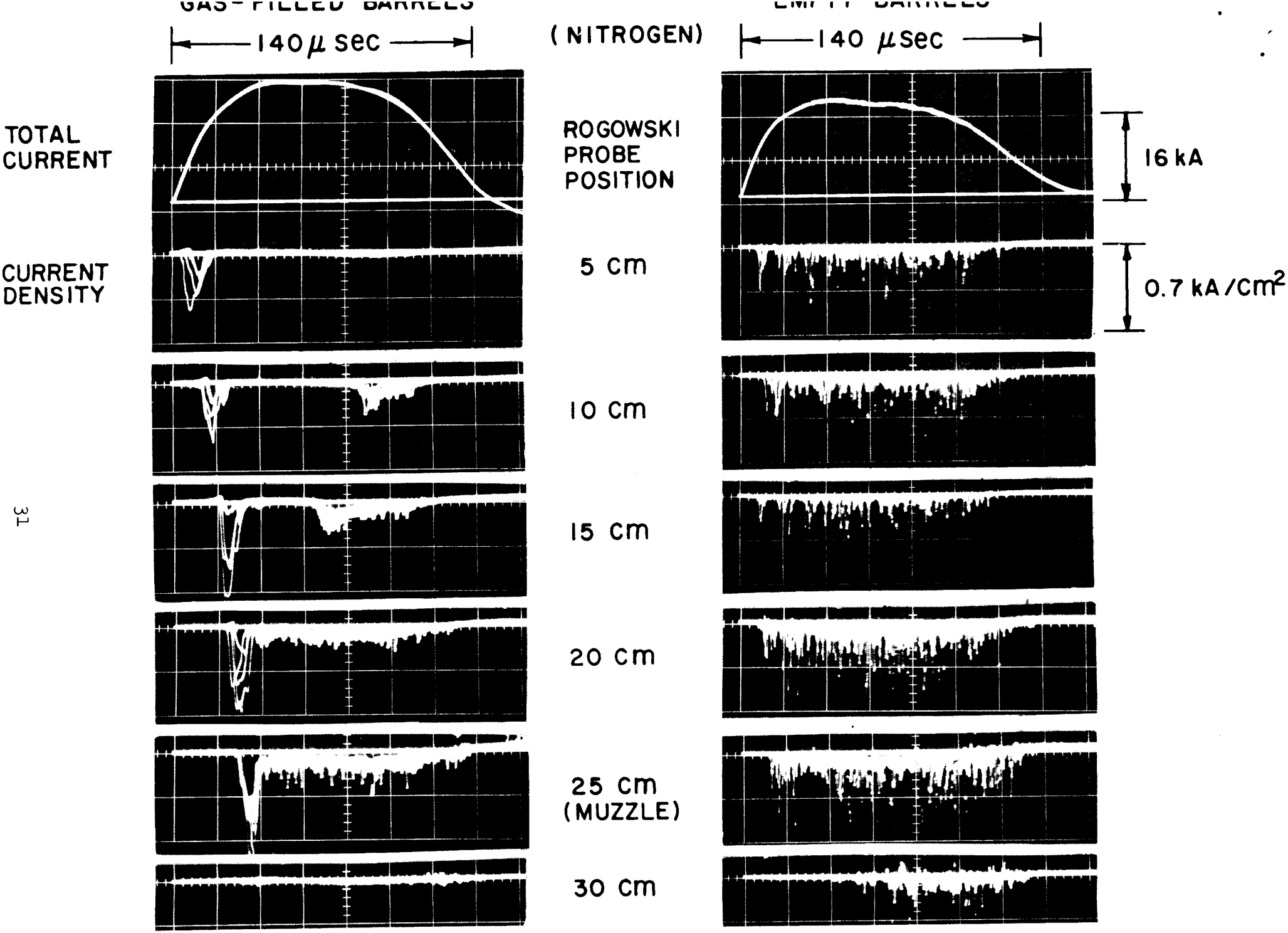

FIG. 15 : ROGOWSKI PROBE OSCILLOGRAMS

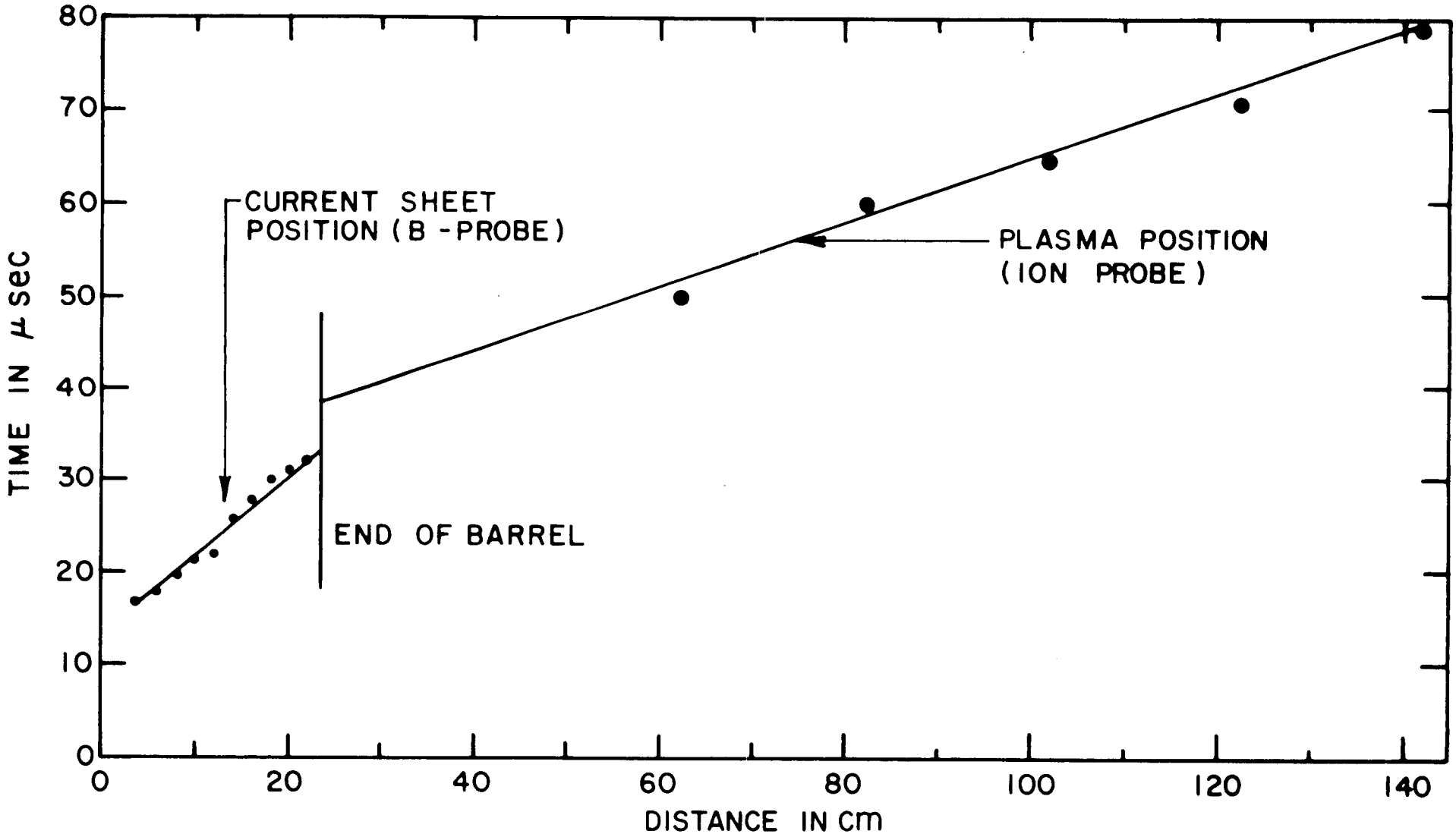

FIG. 16 : SPACE TIME DIAGRAM SHOWING THE POSITIONS OF THE CURRENT SHEET AND THE PLASMA FRONT, NITROGEN PROPELLANT.

produced which travels at 2-3 cm/μsec.

4.2.2 Pulsed Arc Gun with Conical Electrodes

In view of the low efficiencies obtained with the Pulsed Arc Gun using a 3-inch outer electrode it was decided to use an electrode geometry similar to that used in High Performance Arc Jets and Hall Current Accelerators.

The configuration of the first electrode arrangement is shown in Figure 17. An external magnetic field of a few kilogauss can be produced by the coil around the anode. Figure 17 also shows the magnetic field lines from this coil and the flux densities normally used. The coil is supplied from a 24 volt battery which is pulsed on for 60 msec. The discharge is initiated by pulsing gas into the electrode region 30 msec after the magnetic field is switched on. The external magnetic field inhibits breakdown, and to overcome this problem a third electrode is connected to a 0.03 μF capacitor charged between 500 and 1500 volts; breakdown occurs between this ignitor electrode and the main electrodes, thus initiating the main discharge. Originally the ignitor was placed in the cathode tip but greater reliability has been achieved with it in the interelectrode space.

Cathodes of both copper and tungsten have been used with no noticeable change in gun performance, however, erosion was severe with the copper cathode.

A number of changes to the electrode configuration have been made using the gun shown in Figure 17. Initially the coaxial region between the anode and the cathode was not lined with insulator and a radial discharge took place in this region; the plasma output was low

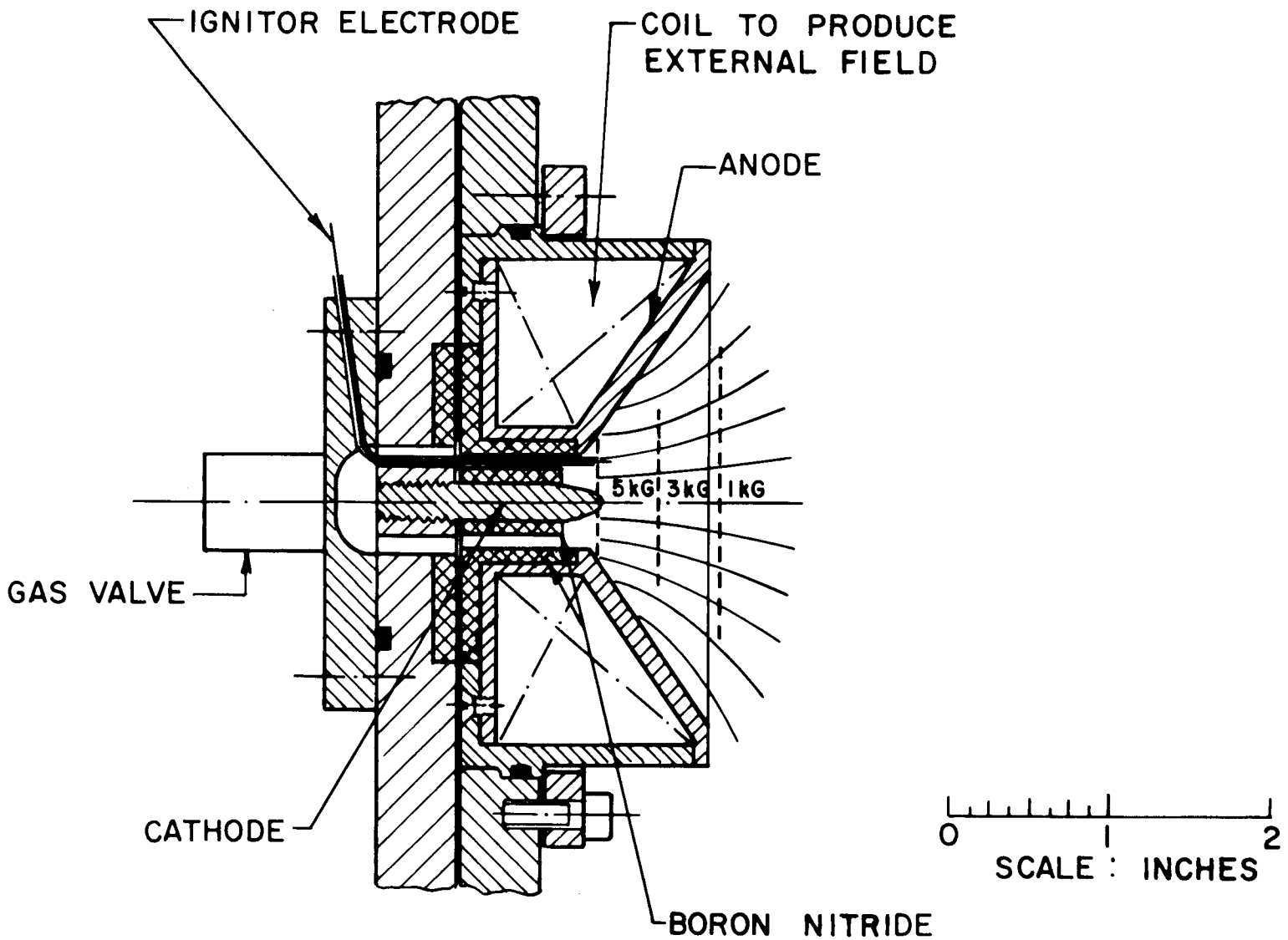

FIG. 17 : PULSED ARC GUN WITH EXTERNAL MAGNETIC FIELD

and severe erosion occurred at the rear end of the anode near the gas input holes. When the coaxial region was lined with insulator, so that the discharge was restricted to the cathode tip and the conical part of the anode, the plasma output increased, but severe anode erosion occurred near the apex of the cone. The cathode tip was moved by lengthening and shortening the cathode assembly with no significant change in plasma output. The presence of the external magnetic field made little or no difference to plasma output but it did influence the onset of tank currents and altered the gun impedance by about a factor of two. A range of magnetic field strength exists where tank currents are least likely; at gun voltages near 100 V, tank currents occur with no external magnetic field, they cease when a field of 5 kG is applied and start again at higher fields. Thermal efficiencies of 15% are typical and the plasma output is similar to that from the gun with the 3-inch diameter anode. Figure 18 shows oscillograms of the output for comparison with Figure 12.

The cone angle of the anode was reduced as is shown in Figure 19. A plot of field lines with this new anode is also shown in Figure 19. Less anode erosion took place, the plasma output increased, and a thermal efficiency of 23% resulted from this change. Figure 20 shows oscillograms of the output from this gun. Again the plasma velocity and gun impedance were similar to those with the 3-inch diameter anode.

Further changes in geometry have been tried. Neutral gas was fed in at the anode, instead of the mid-point between electrodes, and a concave cathode was used. These changes made no significant difference to the plasma output.

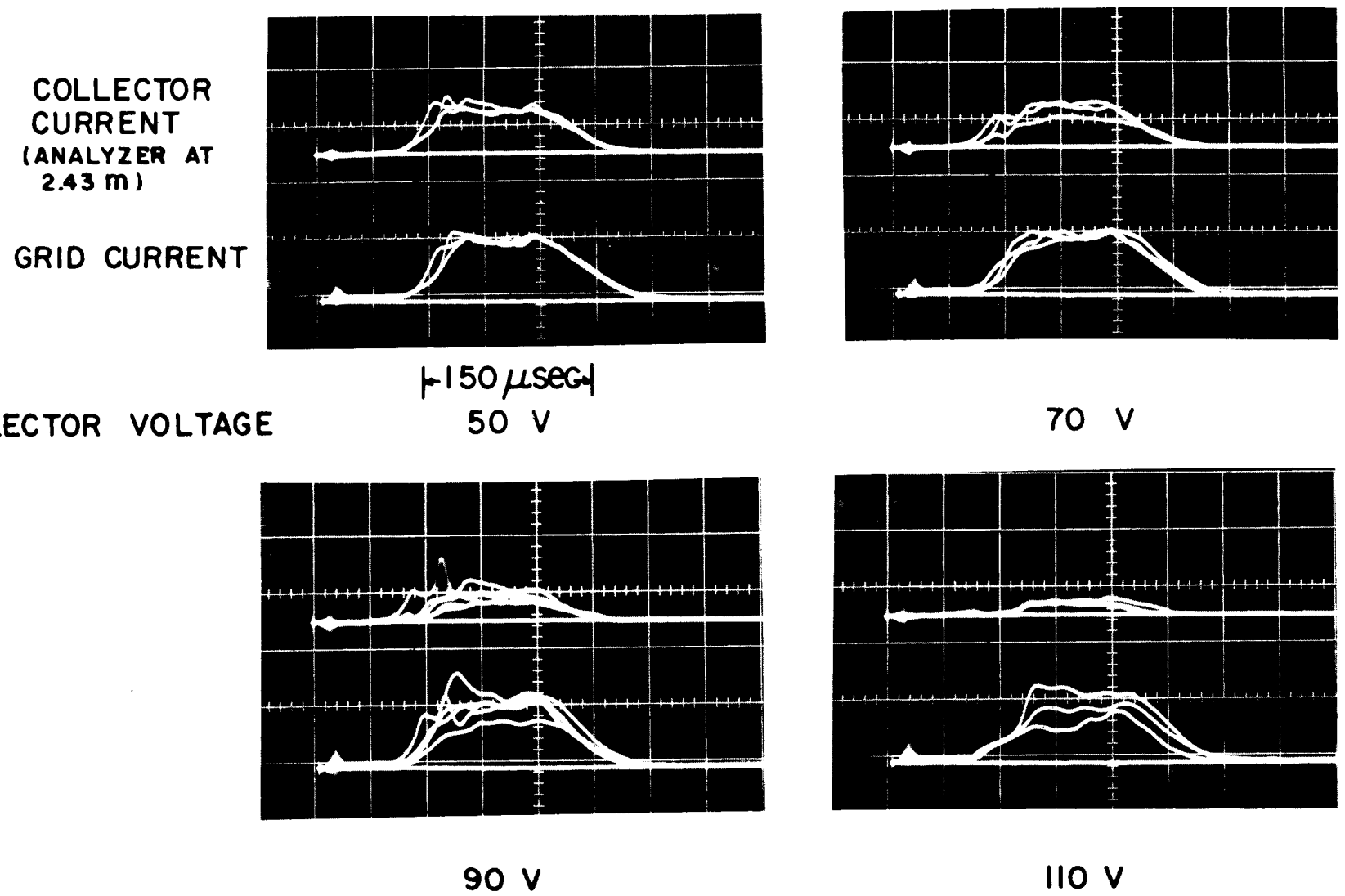

FIG. 18 : ION ENERGY ANALYZER OSCILLOGRAMS, NITROGEN PROPELLANT

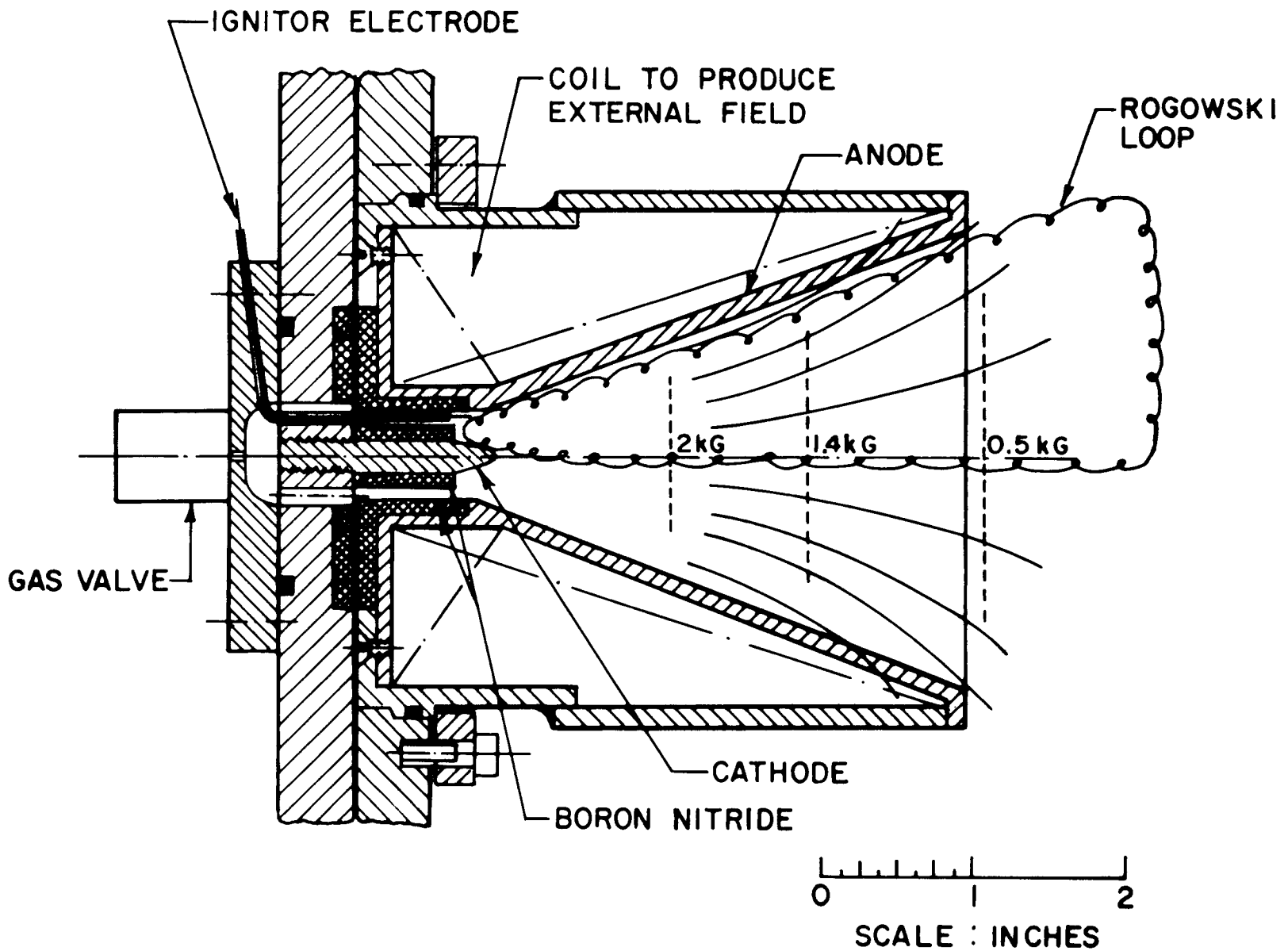

FIG. 19 : PULSED ARC GUN WITH EXTERNAL MAGNETIC FIELD.

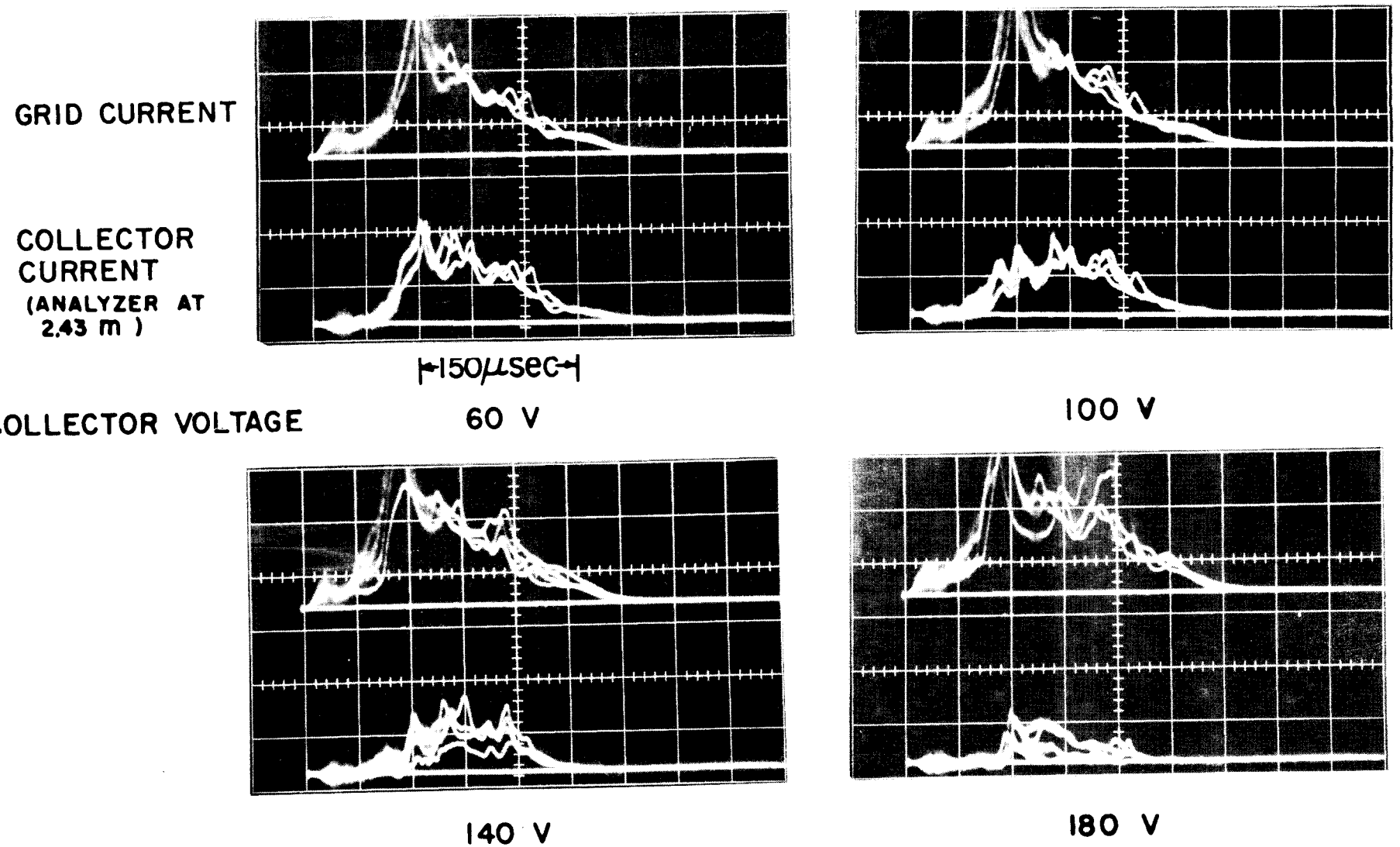

FIG. 20 : ION ENERGY ANALYZER OSCILLOGRAMS, NITROGEN PROPELLAN

Finally the plasma output using nitrogen as the propellant gas was compared with the output when other gases were used. Figure 21 shows the different outputs from the ion energy analyzer when hydrogen, nitrogen, argon and xenon were used as the propellant gas. It is significant that neither the plasma density nor the ion energy alters when hydrogen, nitrogen or argon is used; in addition the plasma output is insensitive to the pressure of the gas in the gas-feed system. These results argue that the propellant gas does not constitute a major fraction of the exhaust plasma but acts as a triggering mechanism while the discharge accelerates adsorbed gas or material from the electrodes. The plasma transit time and ion energy given by the gridded analyzer are consistent with an atomic weight of about 15; this fact rules out the possibility that the exhaust consists of electrode material (atomic weight of copper is 64). However, it is possible that material of low atomic number (e.g., nitrogen, oxygen, or carbon) from the residual gas in the vacuum chamber is deposited on the electrodes between shots and subsequently accelerated. The base pressure in the vacuum tank is typically 2×10^{-6} Torr; if this gas is air then the time to deposit one monolayer of 10^{15} molecules per cm^2 is one second. The interval between shots of four seconds is long enough for 8×10^{17} molecules to be deposited on the anode (area 140 cm^2); this figure is comparable with the total number of ions in the exhaust (of the order 10^{18}).

The exhaust plasma did change significantly when hydrogen was substituted for nitrogen in the 3-inch gun. The above results appear to be characteristic of the smaller gun. Experiments are in progress to determine the effect of adsorbed gas; these include firing at a faster

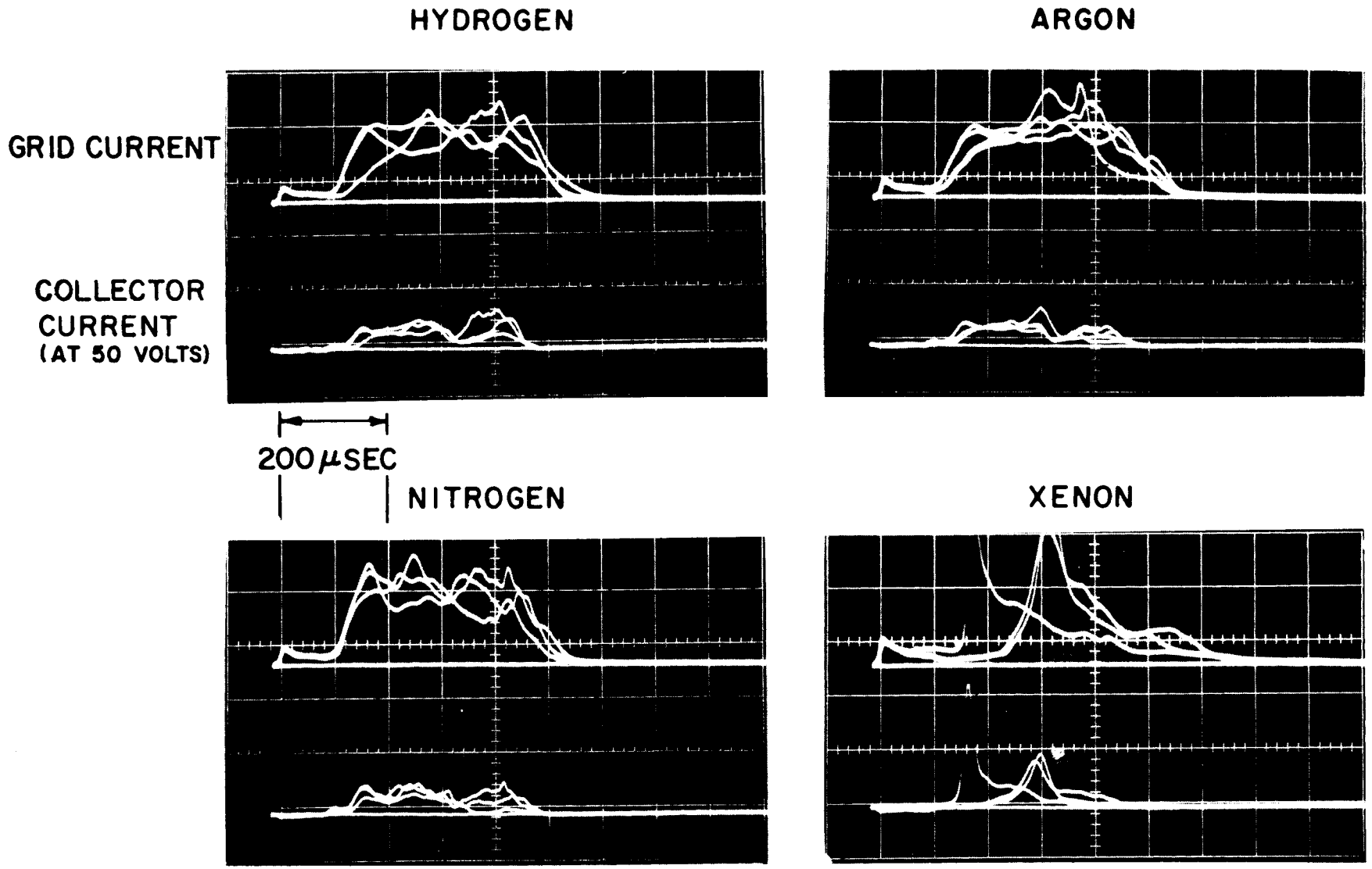

FIG. 21: ION ENERGY ANALYZER OSCILLOGRAMS SHOWING THE EFFECT OF CHANGING THE PROPELLANT GAS (ANALYZER 2.43 m FROM GUN)

repetition rate and redesign of the gas-feed system to allow a higher gas flow rate during the discharge.

5.0 SUMMARY AND DISCUSSION

The program for the past year, as in the previous three years, has been directed toward understanding the important physical phenomena that occur in pulsed plasma thrustors, rather than trying to optimize a particular thrustor configuration. Diagnostic techniques were chosen to give convenient, rapid estimates of thrustor performance: calorimetric efficiency has been used as an upper limit for thrust efficiency and ion velocity has been a measure of I_{sp}. Propellant utilization studies were started late this year and a thrust stand was built so that the propulsion parameters I_{sp} and efficiency, $T^2/2\dot{m}P$, can be measured directly.

The situation of moving current sheet accelerators with uniform mass loading is as follows: the propellant is either entrained by the current sheet or driven into the electrodes; for practical purposes the snow-plow model is adequate to describe the dynamics of the current sheet; if the mass loading and geometry are specified a pulse-line impedance and voltage can be prescribed to give a desired current sheet velocity; the velocity of the plasma expelled from the accelerator is approximately equal to the sheet speed providing that the driving force is maintained until the current sheet reaches the end of the electrodes; thermal efficiencies of the order of 40% can be achieved at exhaust velocities between 2×10^4 and 2×10^5 m/sec.

In summary, we now know how to design and build moving current sheet accelerators for any I_{sp} between 2000 and 20,000 seconds with thermal efficiencies of the order of 40%. No further work is planned on moving current sheet accelerators employing a uniform mass loading because we believe that the efficiency of this type of accelerator is limited to about 50% by radiation losses.

Two ways of improving the efficiency are being investigated; in the one a non-uniform mass loading is employed in order to make the current sheet accelerate continuously and in the other the current distribution is stationary or "quasi-stationary". The former requires a fast gas valve and a high voltage switch in order to obtain adequate control over the neutral gas distribution; these have been developed and measurements are in progress.

The stationary current sheet accelerator or Pulsed Arc Gun looks promising. In principle it has many advantages over the moving current sheet accelerator and these are described in the Introduction. It has two distinct advantages over steady-state thrustors; pulsed arc guns can be operated at a very low average power (a few watts) while at very high peak powers ($\sim$ megawatts) and because propellant is also pulsed, very low ambient vacuum tank pressures can be maintained without gigantic pumping systems. We believe that megnetoplasmadynamic arcs without bias fields can only be efficient at a power level of hundreds of kilowatts; with a bias field this power level can drop to tens of kilowatts. If the physical phenomena active in D. C. accelerators can be duplicated in pulsed systems, then pulsed accelerators can be employed, both in the

laboratory and in space, to study the performance of M.P.D. arcs without the need for very high power levels.

To summarize the preliminary results obtained with pulsed arc guns: a quasi-stationary discharge can be established and plasma is ejected continuously during the pulse; the energy to charge ratio of the ions in the exhaust is less than the voltage at the terminals of the gun; the plasma velocity has been varied over the range 1 to 5 cm/μsec; a bias field improves the symmetry, and reduces the electrode erosion but does not alter the performance significantly; a thermal efficiency of 15% is typical with the present configuration; tank currents are difficult to avoid and when flowing improve the measured efficiency. The neutral gas-feed appears to be inadequate at present; in some cases the discharge operates on adsorbed gases, a problem similar to the entrainment problem in D. C. devices.

The development of the Pulsed Arc Gun is a significant contribution to the field of pulsed plasma accelerators, however, more experiments are required to determine if it can be used as a thrustor.

One further significant accomplishment this year is in the development of energy storage capacitors. Over one million discharges have been achieved at energy densities of 80 joules/lb and 4 joules/in^3 with a charging voltage at 4 kV. These energy densities are considerably higher than required for practical missions; we are confident that neither capacitor weight nor lifetime will be the limiting factor in the performance of pulsed plasma thrustors.

6.0 APPENDICES

Appendix I. Diagnostics

I.1 Ion Energy Analyzer

A simple gridded analyzer which identifies the energy of the ions in the exhaust has been developed. In contrast to the Eubank-type analyzer[6] which was used previously, the new analyzer has much poorer resolution. Its main advantages are compactness, ease of orientation within the vacuum chamber, and adequate performance at the plasma densities and velocities which are encountered in our application.

The analyzer is shown in Figure 22. The grid behind the entrance hole is biased sufficiently negative, so that it repels all the electrons, while the collecting plate behind the grid is given a positive potential so that it accepts only those ions whose kinetic energy satisfies the following relationship

$$1/2\ Mv^2 > ZeV \qquad (8)$$

where V is the positive potential on the collecting plate.

The signal from the first grid varies as the total ion current entering the probe while the collector current is proportional to the current from the fraction of ions which satisfy Equation (8).

Two points about the use of this analyzer should be noted. Firstly, any potential difference between the plasma and the probe will produce a plasma sheath which alters the energies of the incoming ions; this effect, which is common to all analyzers, can be appreciable for low energies particles if the analyzer is too close to the gun. Secondly, the mesh size of the grid must be less than the Debye shielding distance appropriate to the grid voltage and the plasma density.

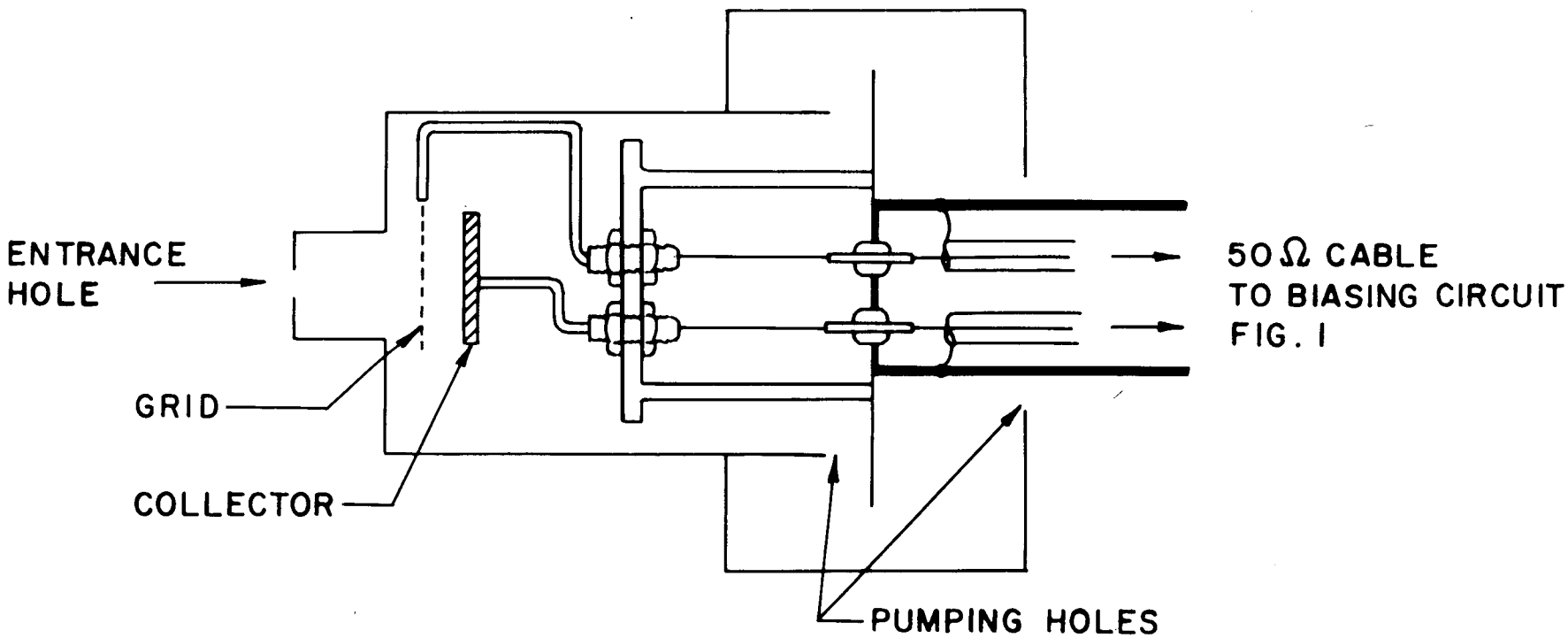

FIG. 22: ION ENERGY ANALYZER

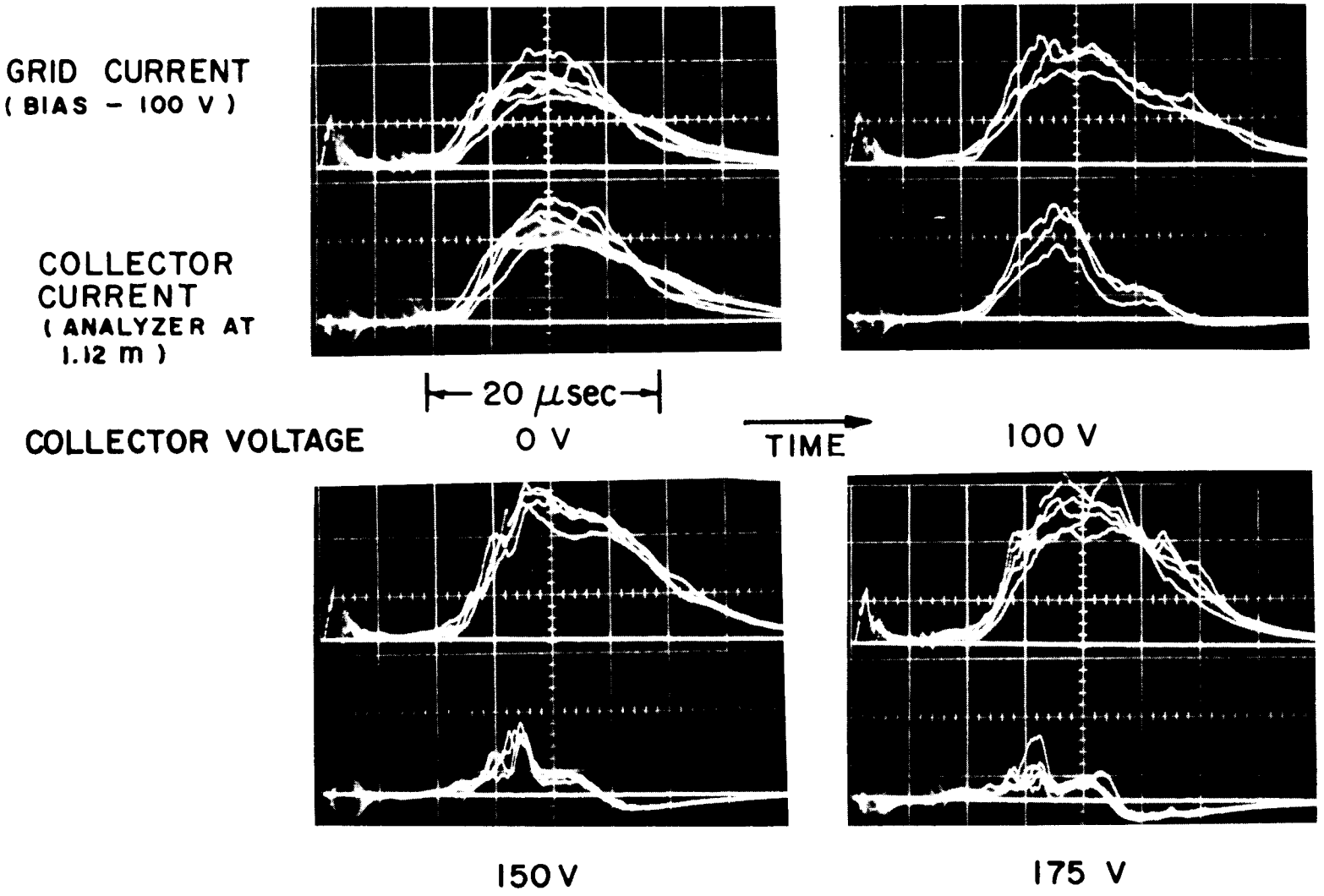

FIG. 23 : ION ENERGY ANALYZER OSCILLOGRAMS

The oscillograms in Figure 23 illustrate the performance of the analyzer. In each picture the upper trace is the current to the negative grid and the lower trace is the current to the positive collector. The current to the collector reduces progressively as its potential is increased. Two marked cut-offs occur which correspond to N^{+} and N^{++} ions. The oscillograms show that approximately 70% of the plasma is doubly-ionized in this case.

I.2 Thrust Stand

A thrust stand of the inverted-pendulum, four-flexure type[7] has been installed in a new vacuum chamber. This vacuum tank, designed for the stand, is four feet in diameter and five feet long. It connects directly into the large chamber through a 16-inch gate valve, allowing operation of the stand at gas flow rates equivalent to 10 shots per second. It can be operated independently of the large chamber, allowing flexibility in the programming of experiments for the two systems.

A four-flexure system was chosen because the degree of criticality of the over-all system is independent of the criticality of each flexure,[8] and because it is possible to load the stand to four times the critical loading before collapse. The first feature means that the location of the center of gravity is not important; this fact greatly increases the versatility and ease of use, and also eliminates the requirement for closely matched flexures; the degree of leveling required is also reduced. The second feature allows operation at or above the critical load, where the mechanical restoring forces are zero, and makes the suspension relatively insensitive to mechanical or thermal drifts.

To eliminate errors due to hysteresis of the flexures, and other non-linear effects, it is desirable to limit the deflection by making the suspension system very stiff. This stiffness is achieved by an electrical feedback network, rather than mechanical means.

The problem of restoring torques from the electrical connections was avoided by making the base of the stand from one-inch thick epoxy board, and carrying the necessary power and electrical signals through the flexures. Thermal problems are avoided by operating at a low duty cycle, with the stand, engine, and capacitors acting as a heat sink.

The complete suspended system, including engine and capacitors, weighs 150 pounds. The flexures are 1.5-inches long by .200-inches wide and .032-inches thick, machined from 321 stainless steel.

A block diagram of the system is shown in Figure 24 and a photograph in Figure 25. A displacement in the stand causes a signal to be induced in the differential transformer (a Sanborn Model FT-1) which is processed through a carrier preamp, then amplified and differentiated. The differentiated signal, which is proportional to the velocity of the stand, is sent through a D. C. power amplifier to one of a pair of coils. The coils are rigidly attached to the base, and surround but do not touch a permanent magnet mounted to the movable portion of the stand. This system provides electromechanical damping, and the over-all Q of the system can be varied easily. The undifferentiated signal is amplified and applied to the second coil, together with a manually applied D. C. voltage, to compensate for drift.

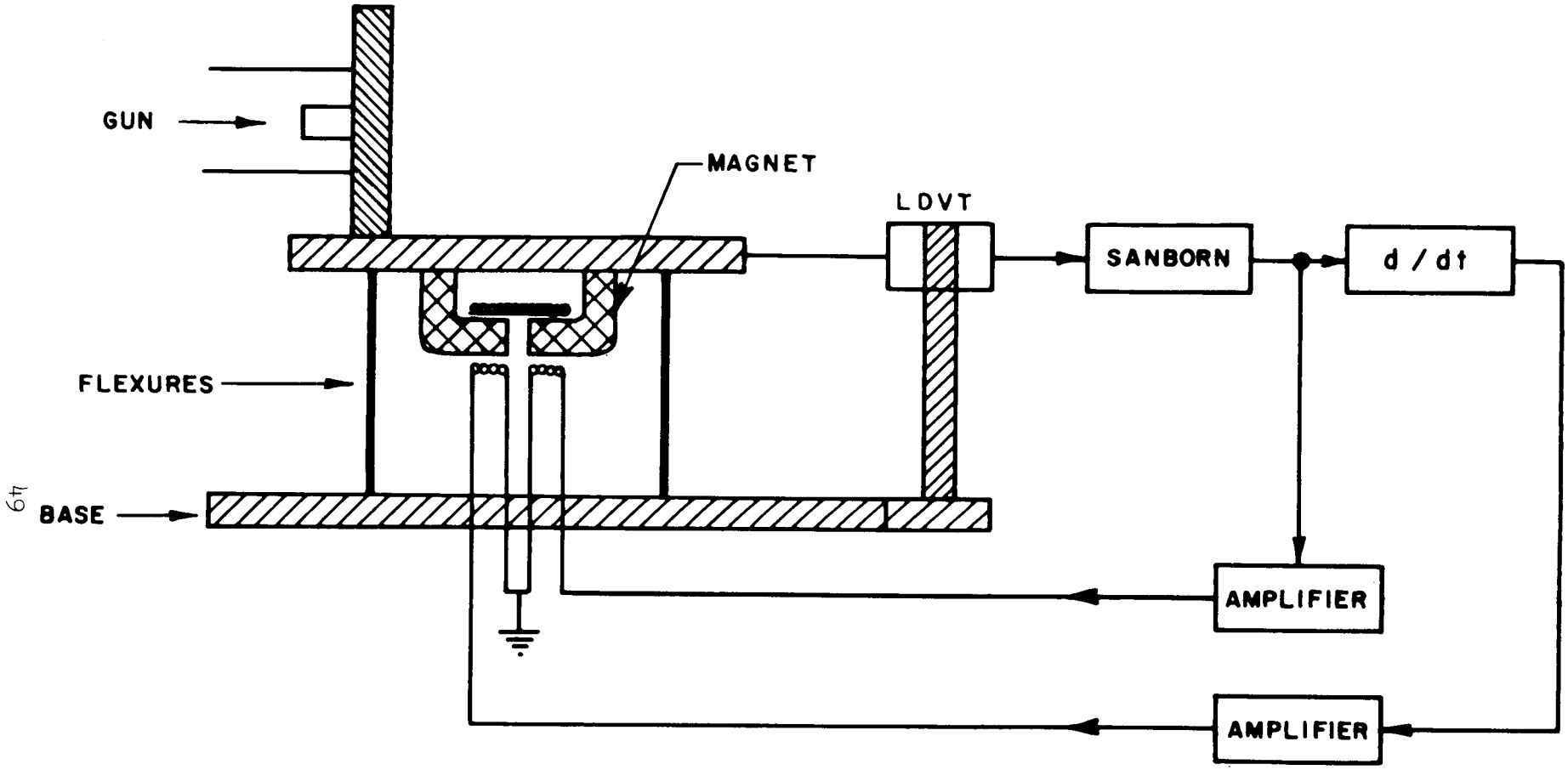

FIG. 24 : THRUST BALANCE FEEDBACK NETWORK

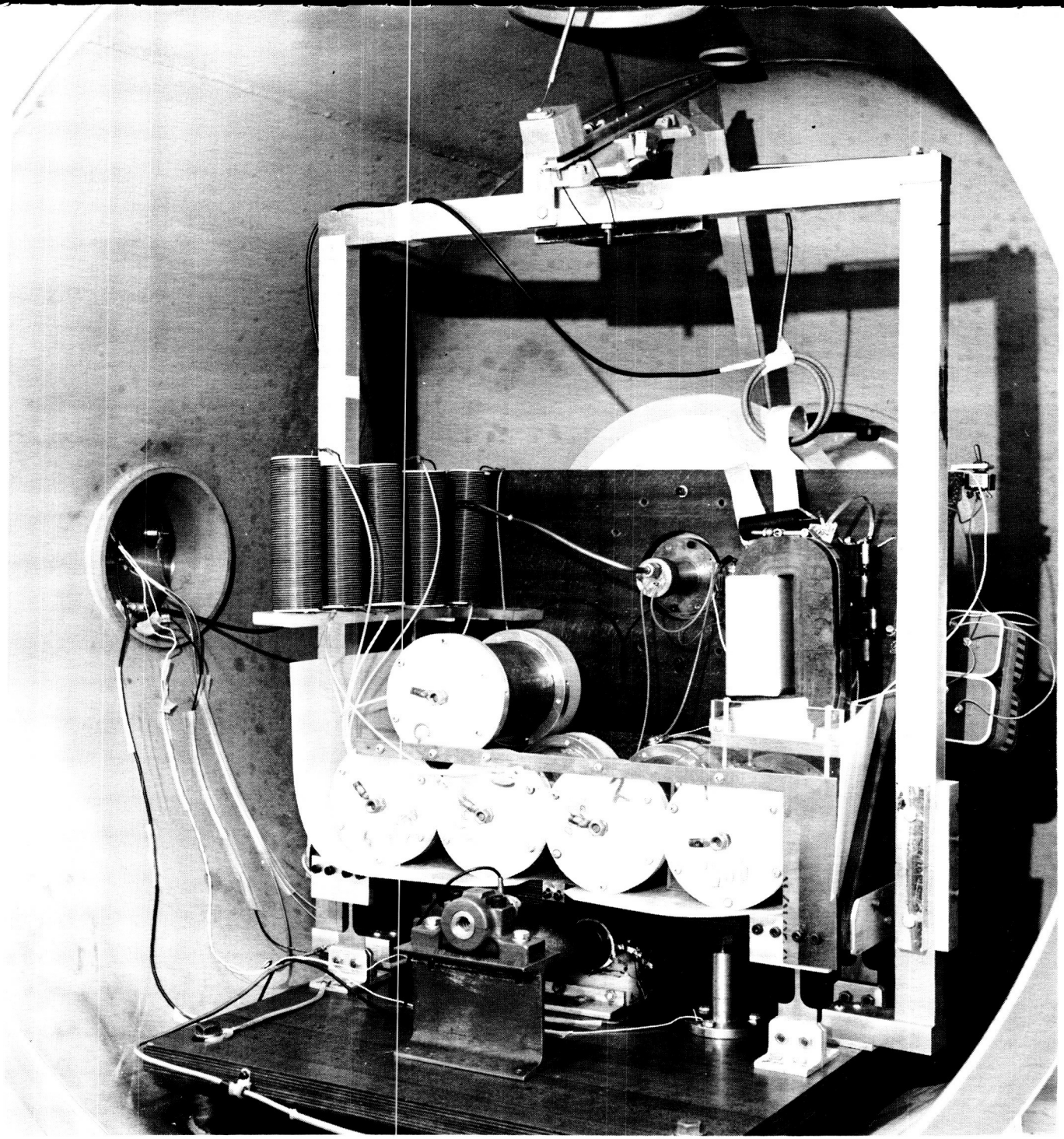

FIG. 25 : PULSED ARC GUN AND THRUST STAND.

The background mechanical noise level is well below 0.1 millipound, and electrical noise due to operation of the gun is not detectable. No corona has been observed at voltages up to 2.5 kV, if the tank pressure is below 10^{-5} Torr. No displacement signal is induced when the gas valve is pulsed with no gas in the plenum. No quantitative measurements of thrust have been made so far but there are indications that the suspension is sensitive to single pulses.

Mass flow rate measurements will be undertaken as soon as all other portions of the system are operating routinely.

Appendix II. Energy Storage Capacitors

About two years ago a capacitor development program was initiated because the capacitor manufacturers would not support an extensive R & D program to develop a lightweight, compact, low inductance capacitor. Our program has been successful and has allowed us to keep pace with the changes and demands of the various accelerators.

The first unit fabricated was a 22 μF, 10 kV capacitor built in the form of a torus; the method of construction employed was such that this capacitor behaved as a pulse-line with an impedance of 17 m Ω and a pulse-time of 0.8 μsec.[3] Since then 12 pulse-lines have been constructed, with impedances between 4 and 45 m Ω and pulse-times from 0.3 to 10.0 μsec; one of these lines can deliver 10^6 amps with a rise-time of 10^{-7} secs into a short circuit load.

For the last four years there has been a steady progression toward lower voltage, higher capacitance (or equivalently longer pulse-time) energy storage capacitors for the various accelerators. For example, in the first accelerator a 1 μF, 20 kV capacitor was used; this was followed by a system with 5 μF at 15 kV, then 10 μF at 10 kV, 20 μF at 6 kV, 180 μF at 3 kV and finally ~ 2000 μF at 500 volts for the Pulsed Arc Gun. To keep abreast of these changes we have studied the properties of dielectric materials and maintained a testing program in order to design optimum systems over a wide range of capacitance and voltage.

To minimize costs all testing has been done on small sample capacitors typically 5 μF each. Using Mylar film for the dielectric

we have obtained lifetimes of the order of 10^6 shots at energy densities of 80 joules/lb and 4 joules/in.^{3} at an applied voltage of 4 kV. This energy density is considerably higher than necessary for a prototype engine and it is apparent now that neither capacitor weight nor lifetime will be the limiting factors in the design of pulsed-plasma thrustors.

The Pulsed Arc Gun operates at very low voltage, typically 150 volts; high energy density film-foil capacitors cannot be fabricated at these low voltages because the minimum film thickness available is 0.00015-inch and several layers have to be used to avoid pinholes. In principle either electrolytic or ceramic capacitors can be used. However, electrolytics do not have adequate reliability, are lossy, and cannot handle the discharge current, and ceramics would be prohibitively expensive for laboratory applications. Ceramic capacitors could be used in the final system.

The most convenient way to fabricate a lightweight energy storage system for the Pulsed Arc Gun is to use a high impedance, high voltage pulse-line and a pulse-transformer. The impedance of the Pulsed Arc Gun is ~ 30 m Ω; therefore, with a 10:1 transformer a lumped parameter line with an impedance of 3 Ω can be employed. A typical line consists of 5 capacitors, each 7 μF charged to 3 kV; the terminal voltage at the gun for a matched load is then 150 volts. Such a system stores 158 joules and weighs 15 lbs, of which 10 are in the transformer. The design and construction of the pulse-transformer are described in the following appendix.

Appendix III Pulse-Transformer Design

A pulse-transformer has been designed to couple the Pulsed Arc Gun to its energy storage system. This step is necessary because the thrustor operates at low voltage and because film-foil capacitors cannot be fabricated with good weight efficiency at voltages less than 2 to 3 kV.

Assuming that the thrustor operates at 150 volts and 0.03 ohms impedance, and that the pulse-line energy source must be charged to 3 kV (thus producing 1.5 kV output into a matched load), we arrive immediately at a turns ratio requirement of 10:1, and a line impedance requirement of 3 ohms. We will discuss first the elementary theory of the pulse-transformer, then the design constraints imposed by our system, and finally the test results from a laboratory prototype.

III.1 Theory

The electrical circuit being considered here is the following,

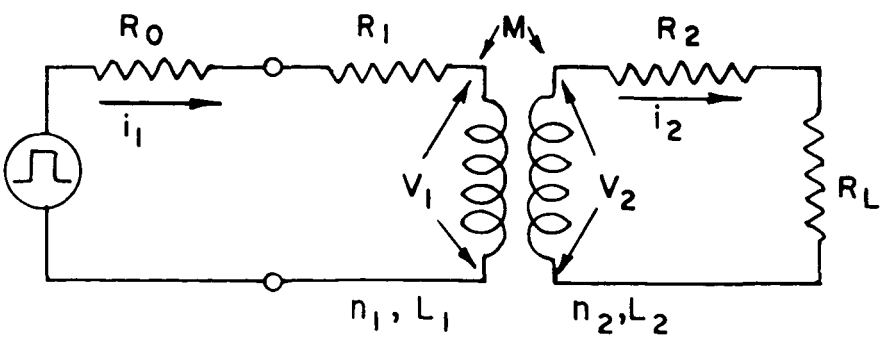

where we characterize the energy source as a zero impedance square-wave voltage generator in series with R_o, the characteristic line impedance.

Here, we define the following parameters:

R_o = pulse-line impedance (pure resistive)

R_L = load impedance (assumed resistive)

n_1 = primary turns

n_2 = secondary turns

L_1 = primary inductance (for $i_2 = 0$)

L_2 = secondary inductance ($i_1 = 0$)

R_1 = primary resistance

R_2 = secondary resistance

k = coupling coefficient

M_1 = mutual inductance referred to the primary ($= KL_1$)*

$n = n_1/n_2$ = turns ratio

We first write the usual voltage relationship which is, for a perfect transformer ($k = 1$, $R_1 = R_2 = 0$)

$$v_2 = v_1/n \ .$$

Since the transformer is assumed lossless,

$$V_1 \, i_1 = V_2 \, i_2 \ ;$$

hence,

$$i_2 = n \, i_1 \ ,$$

and

$$\frac{V_1}{i_1} = n^2 \frac{V_2}{i_2} = n^2 \, R_L \ .$$

*Here, $M_1 = nM$, if $M \equiv k\sqrt{L_1 \, L_2}$, as is the usual definition.

We thus define a "reflected" impedance $R_L' = \frac{V_1}{i_1} = n^2 R_L$. (The requirement for a 3 ohm line now follows from the 10:1 turns ratio, and R_L = 0.03 ohm). By similar reasoning, we have

$$L_2' = n^2 L_2 ,$$

and

$$R_2' = n^2 R_2$$

It is now convenient to draw the "equivalent circuit" of the transformer in terms of what is seen at the primary terminals; we follow the procedure of Bostick:[8]

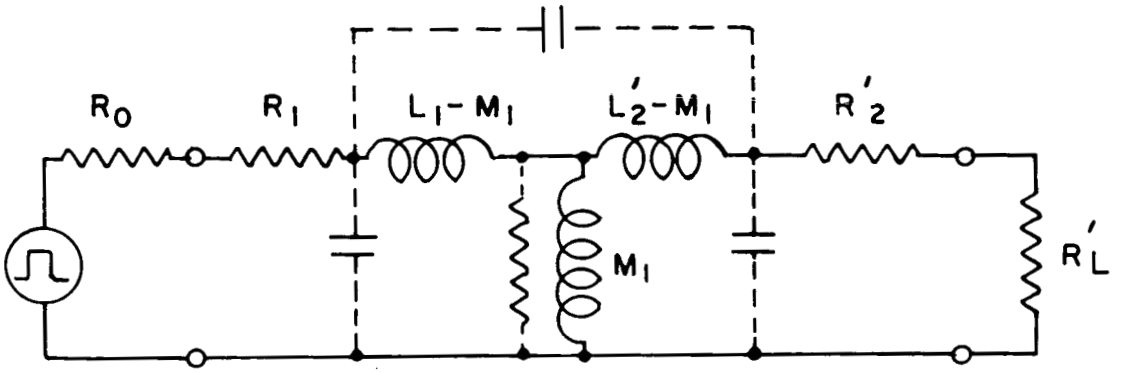

The additional circuit elements, e.g., shunt resistance and capacitance as shown in dashed lines, are not important at the relatively low frequencies we employ, and so are neglected. (Fine lamination of the core reduces the core eddy-current loss to a negligible level.)

One further approximation which is quite accurate here is that $\frac{L_1}{L_2} = n^2$, since both coils are closely wound on the same core. Then $L_2' = L_1$, and the equivalent circuit becomes, taking $M = kL_1$,

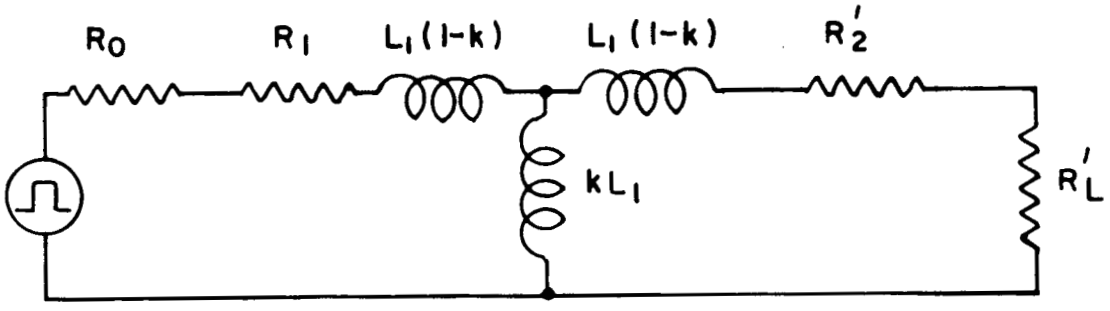

We are now in a position to place limits on the transformer parameters which are dictated by the load impedance R_L, the voltage V_1 on the primary, and the duration τ, of the pulse. These are:

(1) The rise-time τ_r of the current through R_L should be much less than τ. We say, arbitrarily, that we require $\tau_r < \frac{\tau}{f}$, (where f is a number somewhat larger than unity.) But (for $1 - k \ll 1$)

$$\tau_r = \frac{2L_1 (1-k)}{R_o + R_1 + R_2' + R_L'} .$$

Now, since efficient operation requires that R_1 and $R_2' \ll R_L'$, and impedance matching requires that $R_L' \simeq R_o$, this simplifies to a requirement

that

$$\tau_r = \frac{L_1 (1-k)}{R_o} < \frac{\tau}{f} .$$

Thus we need good coupling, and L_1 not unnecessarily large.

(2) The necessary size of L_1, however, is given by the requirement that the shunt impedance of kL_1 should not drain off an important fraction of the input current during τ. We associate with this current drain a rise-time $\tau_s = L_1/(R_o+R_1) \simeq L_1/R_o$, and will require arbitrarily that $\tau_s >> \tau$, or specifically that

$$\tau_s \left(\simeq \frac{L_1}{R_o} \right) > f\tau ,$$

where as before f is a number greater than the order of one.

Combined, these two criteria demand that

$$f < \frac{L_1}{R_o \tau} < \frac{1}{f(1-k)} ,$$

and in particular, that

$$f^2 < \frac{1}{1 - k} .$$

Here, we find, for example that for f = 5, we must have a coupling coefficient of 0.96 or better. Such a value is obtainable, however, and we will set as a preliminary requirement

$$L_1 = 5R_o\tau$$

(3) The core must not saturate. If it does, L_1 drops to a very low value, as does k, and the load is immediately decoupled from the pulse-line. To derive the criterion for satisfying this condition,

we recall from Maxwell's equations that

$$\int E \cdot d\ell = - \frac{\partial}{\partial t} \int B \cdot dA = - \dot{\phi} ,$$

or, that

$$\frac{V_1}{n_1} = - \frac{A}{\tau} \Delta B ,$$

where A is the cross-sectional area of the core. Obviously, we must have

$$\Delta B < B_{max} \qquad (\text{if } B = 0 \text{ at } t = 0),$$

and so the area requirement on the core is

$$A > \frac{V_1 \tau}{n_1 B_{max}}$$

The task of the designer is now to reconcile these requirements while making the transformer as light and efficient as possible.

To study in detail the optimization of transformer design, we assume the use of a double "C" core, which has the primary wound on one leg and the secondary on the other. The two windings are assumed to have identical volumes and to fill the "window". We further assume that the core has a square cross section. Figure 26 shows the configuration with the designation of various dimensions by appropriate symbols. Our procedure now will be to express the various constraints in terms of this geometry and then to attempt to arrive at an optimum design.

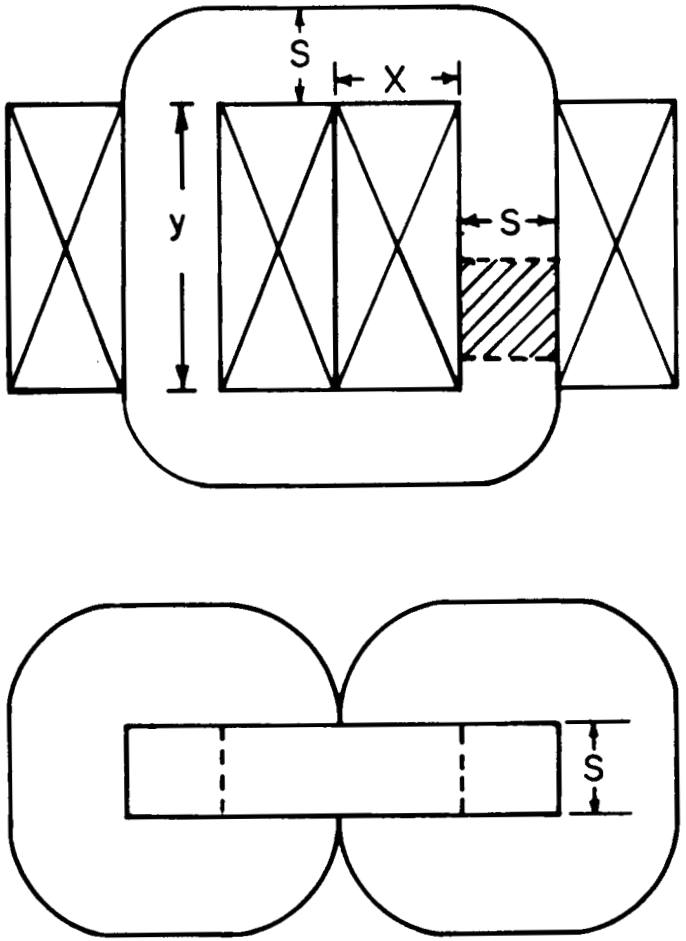

FIG. 26 : CONFIGURATION OF TRANSFORMER CORE AND WINDING.

First, the core area requirement is

$$A(= S^2) > \frac{V_1 \tau}{n_1 B_{max}}$$

To minimize weight, we make this an equality, and so

$$n_1 S^2 = k_1, \qquad \text{where} \quad k_1 = \frac{V_1 \tau}{B_{max}} \quad . \tag{1}$$

Next, there is the compromise time constant requirement that $L_1 = 5\ R_o \tau$. For a non-saturated magnetic circuit of uniform cross-sectional area A and length ℓ,

$$L = \mu n^2 \frac{A}{\ell} \quad ,$$

where n is the total number of turns, and μ is the effective core permeability, including the effect of gaps. We measure ℓ along the center of the cross section, and obtain

$$n_1^2 \frac{S^2}{2(x+y) + \pi S} = k_2 \quad , \tag{2}$$

where

$$k_2 = \frac{5 R_o \tau}{\mu} \quad .$$

In estimating efficiency, we neglect core losses, and concentrate on ohmic winding losses. This is a very safe procedure at the frequencies contemplated in our applications.

If j is the current density in the winding, η the average or specific resistivity of the winding, and V_w the coil volume, then the power loss is

$$P = j^2 \eta\ V_w \quad .$$

But

$$j = \frac{n_1 I_1}{xy} ,$$

and

$$V_w = y[4xS + \pi x^2] ,$$

so

$$P = I^2 R_1 = I^2 \cdot n_1^2 \eta \left[\frac{4S}{xy} + \frac{\pi}{y}\right]$$

Efficiency may be defined now as

$$\epsilon \equiv \frac{R_o}{R_o + 2R_1} ,$$

since each winding, irrespective of turns ratio, reflects a series resistance R_1 into the primary terminals.

Thus,

$$\epsilon = \frac{1}{1 + k_3 n_1^2 \left[\frac{4S}{xy} + \frac{\pi}{y}\right]} \tag{3}$$

where

$$k_3 = \frac{2\eta}{R_o}$$

Finally, the transformer mass is

$$M_e = \rho_c S^2[2y + 4x + \pi S] + 2\rho_w xy[4S + \pi x] \tag{4}$$

where ρ_c and ρ_w are respectively the densities of core and coil.

Now, one may gain an insight into requirements for efficiency by using Equations (1), and (3) to eliminate n_1; the result is

$$\frac{1}{\epsilon} = 1 + \frac{k_1^2 k_3}{S^4 y} \left[\frac{4S}{x} + \pi\right] , \tag{5}$$

and we obviously wish to make the second right-hand term in Equation (5) less than unity. One notices that this term is dominated by the factor $1/S^4$; the ratio S/x will not ordinarily cover a wide range of values and y itself will be expected to remain within certain reasonable bounds. This is to argue, then, that Equation (5) together with k_1 and k_3 determined from external requirements, allows a fairly close first estimate of the minimum acceptable S. Let us take the example of:

$$V_1 = 1500 \text{ volts}$$

$$\tau = 150 \ \mu\text{sec}$$

$$B_{max} = 15 \text{ kilogauss}$$

$$R_o = 3 \text{ ohms}$$

$$\eta = 3 \times 10^{-8} \text{ ohm -m.} \quad \text{(includes the effect of winding space factor)}$$

These give

$$k_1 = 0.15$$

$$k_3 = 2 \times 10^{-8} ,$$

for which

$$\frac{1}{\epsilon} = 1 + \frac{4.4 \times 10^{-10}}{S^4 y} \left[\frac{4S}{x} + \pi\right]$$

If we take the brackets equal to 10, and the whole second term equal to unity (50% efficiency) we obtain

for $y = S$, $S = 2.1$ cm

for $y = 3S$, $S = 1.7$ cm

for $y = 10S$, $S = 1.3$ cm.

It is clear then, that the core leg will probably have to be more than 2 cm on a side.

The core volume, however, is obtained simply and directly by combining Equations (1) and (2) so as to eliminate n_1;

$$\frac{k_1^2}{S^2[2(x + y) + \pi S]} = k_2 \ , \tag{6}$$

or,

$$V_c = \frac{k_1^2}{k_2} \ .$$

Now, we must guess at an effective μ in order to obtain k_2; if we let $\mu = 100$, then

$$k_2 \simeq 20 \ ,$$

and $V_c \simeq 1.1 \times 10^{-3}$ m^3, which corresponds to a mass of about 9 kG.

If B_{max} = 17 kilogauss, and τ = 100 μsec, the core mass drops to a little over 5 kG.

It is interesting to note that if μ is increased, the core volume V_c also <u>increases</u> according to the criteria of Equations (1) and (2), and Equation (6). One may see how this occurs through the following hypothetical sequence of changes. First, suppose that for a given core configuration and winding we increase μ. This has the effect of increasing L_1, and so, in order to bring L_1 back to its predetermined value, n_1 must be decreased. This decreases $V_1\tau$, however, since it depends only upon B_{max} and not μ, and so the core cross section must be increased to restore $V_1\tau$. Implicit in all this is the assumption that the coupling coefficient k remains constant with the change in μ. In

fact, the dependence is very close to $(1-k) \sim \frac{1}{\mu}$ if the core is not approaching saturation. Now, if we note that

$$k_2 = \frac{fR_o\tau}{\mu} ,$$

where up to now we have guessed that f = 5, but where actually, as shown earlier

$$f = \frac{1}{\sqrt{1 - k}} ,$$

we see that

$$k_2 = \frac{R_o\tau}{\mu} \cdot \frac{1}{\sqrt{1 - k}} \sim \frac{R_o\tau}{\sqrt{\mu}} ,$$

and so, this improved approximation still requires an increase of V_c with μ, although not as rapid.

One may inquire as to the possibility of going to even much lower values of μ than 100, perhaps even to an air core. The answer is simply that in this limit, the required coil weight and volume would become unacceptable.

An independent benefit of working at moderate μ is that a core gap which reduces effective circuit μ to the order of 100 (when the actual core material may be a hundred times higher) has the effect of closing up the core hysteresis loop, or reducing the remnant B when H has returned to zero from an excursion of a single sign. Thus, much greater ΔB is available than would be for a gapless core.

These considerations provide a starting basis for design of an operational pulse transformer. A thorough analytic optimizing through solution of Equations (1)-(4) in the given variables appears to be less

practical than a "trimming" procedure which employs as a starting point a core configuration selected by the foregoing approximate means.

III.2 Experiment

Preliminary testing of a transformer (Figure 27) wound on (an Arnold AL 1729 A 2 mil Silectron C) core has been completed, and performance has proved quite satisfactory. The core dimensions are:

$$S = 3.7 \text{ cm},$$

$$x = 3.7 \text{ cm},$$

$$y = 7.5 \text{ cm}.$$

$$n_1 = 100 \text{ turns}$$

$$n_2 = 10 \text{ turns}$$

The windings were of copper foil of 3" width, .0008" in the primary, and 0.010" for the secondary. The important distinction between this transformer and the assumptions of the foregoing analysis is that the windings did not fill the "window" of the core. In order to assure tight coupling, half of the primary and half of the secondary were wound on each leg.

In these tests, a pulse-line energy source of 3 ohms was used. It was built in eight sections, each of which had 4 μfd capacitance and 36 μh inductance, except for first and last mesh inductance of 18 μh. The total pulse-time was 250 μsec.

A dummy load of 0.03 Ω was used for initial tests. No saturation of the core was noticed for V_1 below 10^3 volts; this limiting value agrees exactly with an assumed B_{max} of 1.7×10^4 gauss. Voltage and current waveforms are shown in Figure 28. Energy transfer efficiency, as calculated from voltage and current waveforms, was 88% with the 12%

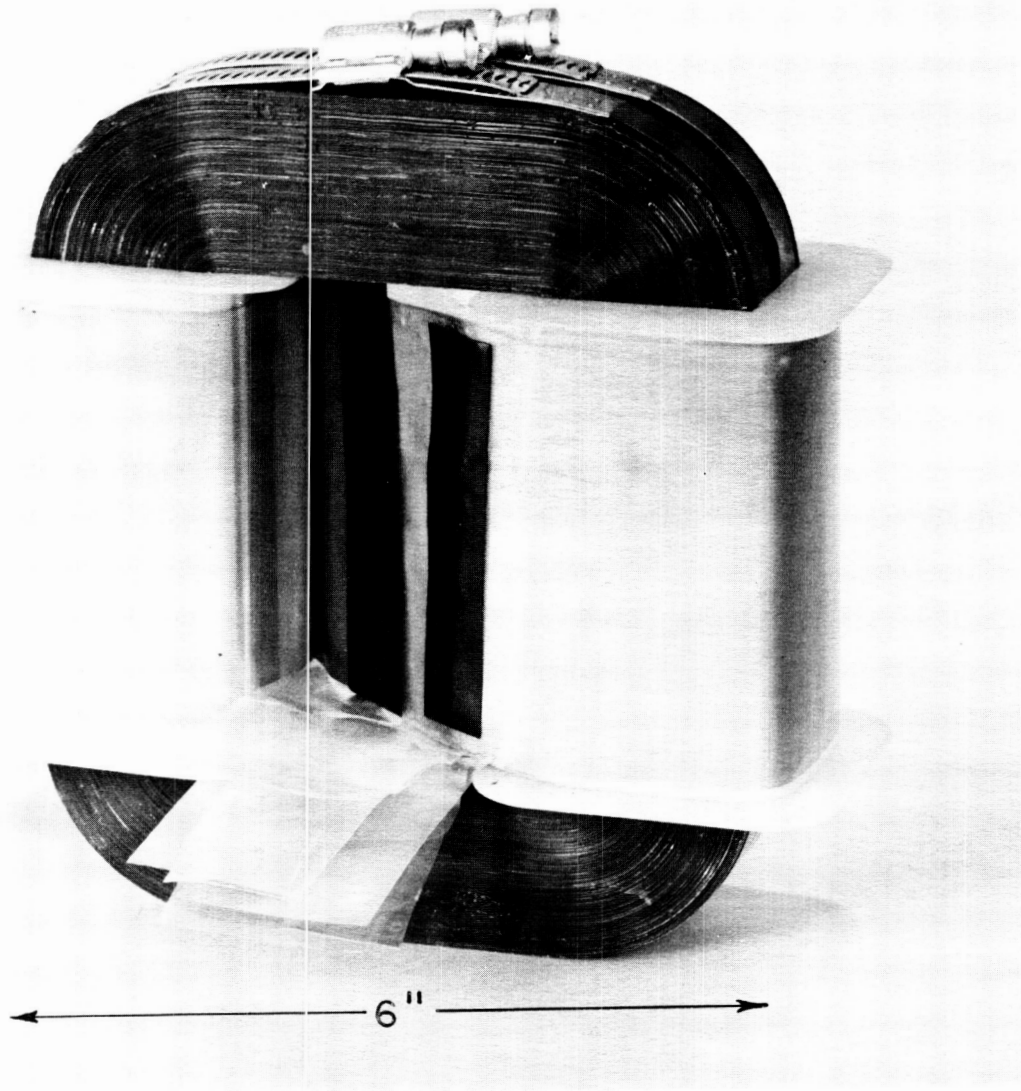

FIG. 27 : PROTOTYPE TRANSFORMER

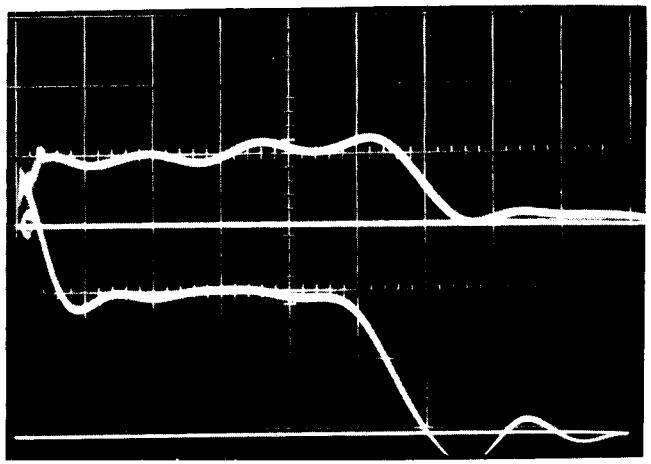

I : 0.305 ka / cm

PRIMARY

V : 500 V / cm

← 250 μsec →

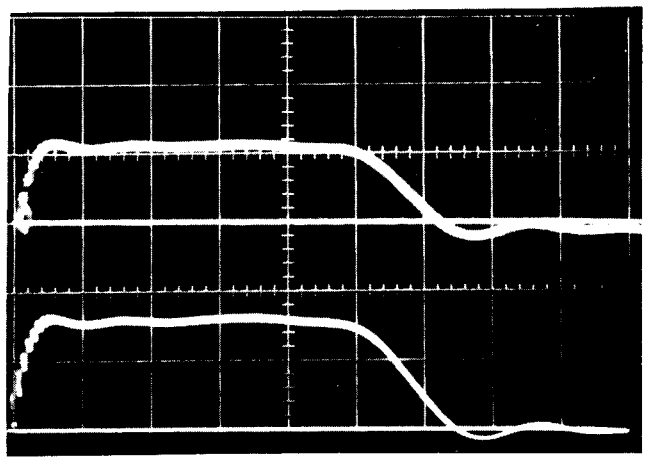

I : 3.05 ka / cm

SECONDARY

V : 50V / cm

FIG. 28 : CURRENT AND VOLTAGE WAVEFORMS FOR THE PULSE TRANSFORMER, 3Ω PULSE LINE INTO A 30 mΩ RESISTIVE LOAD.

loss being entirely attributable to the high secondary resistance of $\sim 0.005\ \Omega$.

Operation of the transformer into an actual thrustor load appeared to be straightforward in that good pulse waveforms were obtained. However, this part of the experiment had difficulties arising from excessive connection resistance between the transformer and load which reduced the energy transfer efficiency to about 50% (Note Fig. 29). Breakdown of the thrustor was hard to achieve at low voltages, although this was remedied by the direct capacitive coupling of a small part of the primary pulse to the thrustor to achieve a "spark plug" function. Figure 29 shows thrustor waveforms. The primary voltage and current were 750 V and 268 A; the secondary values were 48 V and 1950 A. The result of some mismatching and I^2R loss is evident here.

It appears that, with careful transformer design and close attention to secondary circuit connections and conductor sizes, efficiencies in the 90% range should be attainable. This work is continuing.

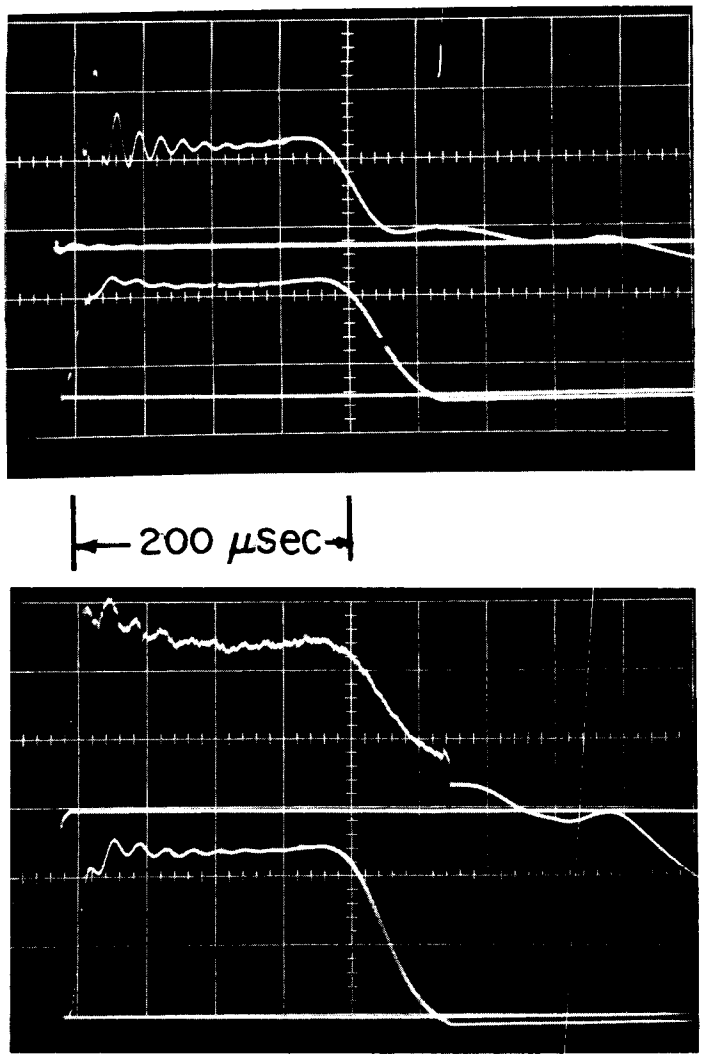

FIG. 29 : THRUSTOR VOLTAGE AND CURRENT WAVEFORMS, THRUSTOR OPERATING WITH PULSE TRANSFORMER AND 3Ω PULSE LINE.

7.0 REFERENCES

1. Lovberg, R. H., Hayworth, B. R., and Gooding, T. J., "The Use of a Coaxial Gun for Plasma Propulsion," Final Report, Contract NAS 5-1139, GD/Astronautics Report No. AE 62-0678, dated May 1962.
2. Gooding, T. J., Hayworth, B. R., and Lovberg, R. H., "Development of a Coaxial Plasma Gun for Space Propulsion," Final Report, Contract NAS 3-2501, GD/Astronautics Report No. GDA 63-0454, dated May 1963.
3. Gooding, T. J., Hayworth, B. R., Larson, A. V., and Ashby, D. E. T. F., "Development of a Coaxial Plasma Gun for Space Propulsion," Final Report, Contract NAS 3-2594, NASA Report No. CR 54149, GD/Astronautics Report No. GDA DBE 64-051, dated June 1964.
4. Gooding, T. J., Hayworth, B.R., and Lovberg, R. H., "Instabilities in a Co-Axial Plasma Gun," AIAA Journal, Vol. 1, No. 6, p. 1289 (1963).
5. Fishman, F. S. and Petschek, H., Phys. of Fluids, 5, 632, 1962.
6. Eubank, H. P., R.S.I., Vol. 34, No. 1, Jan. 1963.
7. Conner, R. F. and Hyman, J., Jr., ARS Report 2180-61.
8. Pulse Generators, edited by Glasoe, G. N. and Lebacoz, J. V., McGraw Hill, Chapters 12, 13, 14, 15 by W. Bostick.

8.0 ACKNOWLEDGEMENTS

The authors wish to express their appreciation to C. W. White and A. R. Miller for their technical assistance and to F. Oddo for the illustrations.